Polarized Targets

Third Lecture by Owen Chamberlain
at the
Tsukuba Summer School, July 19, 1972

A great deal of our knowledge of particle physics comes through the observation of scattering processes. To make this information quantitative we measure differential scattering cross sections. But, since many of the particles in which we are interested have spin, it is usually important to have information about the spin dependence of nuclear interactions. We measure this spin dependence either by observing scattering processes of polarized beams, or observing scattering processes on polarized targets, or by observing the residual polarization after a scattering process with initially polarized particles.

I will restrict my discussion of polarized particles to particles of spin 1/2. In this case, the polarization can be represented as a vector whose direction indicates the predominant axis of rotation. Thus, a sample of protons would be said to be polarized upward if the rotation of the protons was predominantly counter-clockwise as viewed from above. This corresponds to the usual right-hand rule. The magnitude of the polarization vector is given by the expression

$$P = \frac{N_{up} - N_{down}}{N_{up} + N_{down}}$$

The number N_{up} represents the number of particles whose spin is up, meaning along the preferred direction in which the polarization is being measured. Correspondingly, N_{down} represents the number of particles whose spin is opposite to the preferred direction. The above expression is suitable for describing the polarization of a beam of particles, or for describing the particles within a polarized target, Clearly, the numerical value of the polarization lies between 1 and -1.

Besides measuring the polarization of beams and targets, we also refer to the polarization in a certain scattering process. For example, we may make reference to the polarization in proton-proton scattering. It is usual to define the polarization in a scattering process as that polarization

which results in the final-state particles when the given collision process is made to occur with unpolarized initial particles. We will be concerned only with strong interactions that conserve parity so the resultant polarization in a scattering process must lie in the direction of the normal to the scattering plane. I define the normal as:

$$\hat{n} = \frac{k_i \times k_f}{|k_i \times k_f|}$$

The conservation of parity tells us that the polarization in a scattering process cannot lie in any other direction, but the component in the direction n may be either positive or negative.

Any elastic scattering process that has a finite polarization in scattering may be used to reveal the polarization of incident particles. Polarization of incident particles would be revealed and measured by observation of the asymmetry in the scattering process. To clarify these statements we may use the example of protons elastically scattered on carbon nuclei. Let us suppose that we have a beam of unpolarized protons moving horizontally and incident upon a carbon target. See Fig. 1. We shall concern ourselves with those protons that scatter at a certain angle to the left at the carbon target. We indicate the scattering angle by θ. After scattering on the carbon target at angle θ, the protons are polarized with polarization P. We suppose that those polarized protons are incident upon a second carbon target and we observe the number scattered to the left at the same angle (θ) as well as the number scattered to the right at angle θ. Because the protons incident on the second carbon target are polarized, there is a left-right asymmetry at the second scattering. We define the asymmetry ε as follows:

$$\varepsilon = \frac{N_{left} - N_{right}}{N_{left} + N_{right}} \quad .$$

It has been shown that the asymmetry ε is equal to the beam polarization which we may here call P_1 $\times$ the polarization at the second scattering, which we may call P_2.

$$\varepsilon = P_1 P_2 \quad .$$

This statement is usually based on arguments involving time reversal invariance.[1] This means that any scattering process that is a good polarizer is also a good analyser of polarization. If we may neglect the energy loss in proton-carbon scattering, we may say that P_1 and P_2 are equal, because the energy and angle of scattering is the same at the first and second targets in our example of Fig. 1. In that case we may say that ε is P^2, and if the experiment described does indeed show more scattering to the left than to the right we say this is evidence of polarization in the scattering process, and except for the sign of P, this may be used as a measure of the polarization in that scattering.

In fact, the polarization in proton elastic scattering on carbon is fairly high and proton-carbon scattering is often used an an analyzer of proton polarization resulting from some earlier scattering process. Thus, we might measure the polarization in pion-proton scattering by scattering pions first on protons, then re-scattering the protons at a second target made of carbon. Observation of the left-right asymmetry in the second scattering could allow us to calculate the polarization induced by the pion-proton collisions, namely, the polarization in pion-proton scattering.

Using the same arguments about time-reversal invariance that are described by Lincoln Wolfenstein in Ref. 1 we may establish an alternate way of measuring polarization in an elastic scattering process. Namely, we may scatter unpolarized beam particles on a polarized target, and observe the resultant left-right asymmetry. An example is shown in Fig. 2. A horizontal beam of pions is incident upon a polarized proton target whose direction of polarization is up, namely out of the plane of the figure. If there is polarization in pion-proton scattering at the angle of observation then it will be revealed by a left-right asymmetry and in fact, the asymmetry will be given by:

$$\varepsilon = P_T \times P,$$

where P_T is the polarization of the target and P is the polarization in pion-proton elastic scattering.

In practice the experiment of Fig. 2 is usually done slightly differently, in order to achieve results of higher accuracy and with reduced systematic

errors. The scattered pions may be measured only with counters on the left, and the right scattered pions, equivalently, can be measured with the left counters by inverting the target polarization. In other words, pions are always counted on the left, but the asymmetry is calculated from the number of scattered pions when the target is polarized up, versus the number when the target is polarized down.

I now want to describe the mechanism by which one can have protons highly polarized. The most common method in particle physics is the method called dynamic nuclear polarization. The method is based very largely on the work of Abragam and Jeffries, and further details may be found in the book by Jeffries.[2] We suppose that we have a sample material that contains, besides protons, some paramagnetic centers that behave somewhat like free electrons, as far as their spin motion is concerned. If this sample is placed in a fairly high magnetic field (about 25 kG) and at a rather low temperature (1°K) then the electrons will be quite highly polarized because of their large magnetic moment. In fact, the polarization of these electrons will be about 88%, even though the protons, with their smaller magnetic moment, will only be polarized by 0.25%. By irradiating the sample with microwaves of the appropriate frequency, we can selectively disturb the thermal equilibrium distribution, and induce high proton polarizations. The situation is described in Fig. 3 (MU32843). The figure shows the four-level system consisting of one proton and one electron. The large energy differences are due to the electron spin interacting with an external magnetic field, and the smaller energy differences are due to the proton orientation. In fact, Fig. 3 is not drawn to scale; δ is only one-thousandth the size of Δ. At thermal equilibrium the lower two levels are about equally populated, and the upper two levels are much less populated. The population ratios are established by the well-known Boltzmann factors. When the sample is strongly irradiated by microwaves whose frequency is appropriate to the transition $\Delta - \delta$, the populations of the states connected by the microwave transition are almost equalized. The populations of the states connected by the transition energy Δ are always given by the appropriate Boltzmann factor, so the electrons continue to have high polarizations. In fact, the obtainable proton polarization is in principle about equal to the electron

polarization. In practice, it is possible to get only 50-60% proton polarization, even when the theoretical maximum is approximately 90%. For the experimentalist, it is important to be able to reverse the target polarization easily. In dynamically polarized targets the polarization may be reversed by shifting the microwave frequency from the frequency $\Delta - \delta$ to the frequency $\Delta + \delta$. Even though the microwave frequency is only shifted by about two parts per thousand, the polarization of the target can be completely reversed.

Figure 4 (MUB-2238) shows the first polarized target magnet built in Berkeley, about 1960. Notice that is is constructed as an H magnet. It would have been better to use a C magnet construction so that the yoke would be in the way only on one side.

Figure 5 (MU-32816) shows the nuclear magnetic resonance signals of protons in a polarized target. The sample in this case was made of lanthanum-magnesium-nitrate doped with some neodymium to give the paramagnetic centers. Part A of the figure shows the nearly symmetrical proton line obtained with a sample at thermal equilibrium. Once the target is highly polarized the signal becomes several hundred times larger and takes on the shape shown in Part B of the figure. Part C of Fig. 5 shows the line shape for a sample highly polarized in the negative direction. When there are no microwaves and the sample is in good thermal equilibrium then the polarization may be computed from the Boltzmann factor. Once the microwaves have been turned on and the target is highly polarized the extent of its polarization can be measured by measuring the area under the proton resonance curves and comparing with the area that was present at thermal equilibrium. The highly polarized samples usually have enhancements of the proton resonance signal by a factor of about 200.

Figure 6 (XBL707-3434) shows the circuit arrangement used to measure the polarization of the target. The rf signal generator is carefully controlled in amplitude and can be changed in frequency on instructions from the computer. The signal generator is coupled through a small capacity (a very large impedance) to the tuned circuit that contains the polarized target sample. The rf voltage induced in that circuit is recorded by an rf amplifier and diode detector that feed a voltage-to-frequency converter (VFC). A gate is turned on for the duration of 100 pulses from the voltage-to-frequency converter, during which time a 100 MHz oscillator is fed into

a fast scaler. The arrangement of the circuit is such that the number recorded in the scaler is proportional to the reciprocal of the circuit impedance. It is this reciprocal circuit impedance which is expected to be linear in the target polarization, to good approximation.

Figure 7 shows the frequency pattern of the Berkeley Polarization Readout System. Four measurements are taken and combined to make one background subtracted point on the display. Two of these frequency settings are within the proton resonance pattern, and one each of background points are taken at a higher frequency and a lower frequency. In Fig. 7 note the sequence numbers 1, 2, 3, and 4, indicating that first a point is taken within the frequency pattern, second a background point on the high frequency side, third a background point on the low frequency side, and fourth another point within the actual resonance pattern. This subtraction procedure is necessary because the basic system itself has a slope in its response with respect to frequency. That is shown graphically on the figure. At the bottom of the figure is shown the resultant proton resonance line after background subtraction.

Figure 8 (XBB707-2983) shows the average of eight successive thermal equilibrium signals. Also shown in the same figure is the background pattern obtained by changing by one percent the main magnetic field. Notice that the background is not a perfectly straight line, but shows considerable curvature. It is necessary therefore to subtract one pattern from the other to obtain the correct area of the thermal equilibrium signal. No such subtraction is necessary for the highly polarized signals because the curvature is quite negligible compared to the large resonance signals obtained for highly polarized targets.

Figure 9 (XBB707-2982) shows a single thermal equilibrium signal at the top of the diagram, with considerable noise visible. Most of that noise seems to come from rounding error in the scaling of the 100 MHz oscillator. The second part of that display shows the average of eight thermal equilibrium signals with much less noise visible. The lower part of the diagram shows highly enhanced signals for both positive and negative polarization, with much reduced gain to compensate for the large enhancement. These resonance peaks were obtained when the polarized target was a sample of butanol. This method of measuring the target polarization seems to be capable of an accuracy of 2% or better.

Figure 10 (MU-30598A) shows the simplest scattering apparatus that has been used in Berkeley with a polarized target. This arrangement was used for the very first run with a polarized target, for elastic pion-proton scattering. Positive pions are incident from the right on the polarized target. A single scintillation counter recorded the scattered pions. A collection of five scintillation counters was used to search out the scattering peak due to pion scattering on free protons. When a pion scattered on a free proton, and when that pion hit the single pion scintillation counter, the recoiling proton hit the center counter of the five proton counters. The intensity of coincidence events involving the other proton counters gave a rough measure of the background due to the scattering of pions on bound protons.

Figure 11 (MUB-10360) shows a more advanced apparatus used for measuring the asymmetry of elastic pion-proton scattering on polarized protons, hence the polarization in pion-proton scattering. Notice there is one array of partially overlapping counters to count the pions and two arrays to count, in coincidence, the protons.

Figure 12 (MUB-12634) shows the raw experimental results in the form of numbers of coincidence counts for a particular proton bin graphed as a function of the pion bin number. Notice the peak in counts near pion bin #9 that is due to the scattering on free hydrogen. The triangles represent one target polarization, the squares represent the opposite target polarization, all for counts that were nicely coplanar in the apparatus. The circles show the results obtained with a dummy target made of heavy elements similar to those in the polarized target but containing no hydrogen. Thus the circles represent the background due to scattering on bound protons in heavy elements. Once the background is renormalized to match the wings of the upper curves a reasonable estimate can be made of the fraction of counts in the peak that are due to free hydrogen, and the remaining fraction to scattering on heavy elements.

Figure 13 (MUB-12294) shows typical results for the polarization in pion-proton scattering at 390 MeV. Data are absent for small scattering angles because the recoil protons then do not have sufficient range to get out of the polarized target satisfactorily. Data are absent near 150° c.m. because the yoke structure of the magnet made it impracticable to obtain those data.

The microwaves are brought to the region of the polarized target by means of a conventional wave guide. The wave guide usually ends in a microwave horn, that is part of the microwave echo box, often referred to as the cavity. In our systems the phrase echo box is more appropriate than cavity because the cavity is not resonant at the applied microwave frequency. The echo box is typically 3 cm × 3 cm × 10 cm long.

Within the echo box there must also be radio-frequency fields that are used for measuring the target polarization. The rf magnetic field is directed down one side of the echo box and up the other side. A conducting septum is placed in the center of the echo box to force the rf field to go fully around the echo box from one end to the other. Figure 14 (MU-34597) shows the calculated pattern of rf magnetic field lines in the lower right portion of the cavity, for an arrangement in which the microwaves are introduced from above. The region of the polarized target sample is at the top of the figure, where the rf field lines are rather equally spaced and therefore the rf magnetic field is of uniform intensity over the sample volume. This assures that a genuine volume average of the polarization is measured by the readout system.

Figure 15 (MU-34598) shows a comparison of proton-proton polarization data by two methods. The data at 328 MeV are obtained using a polarized target. The triangles show the earlier data at 315 MeV obtained with a polarized beam. The good agreement of these results indicates that the target polarization is being measured reasonably correctly. Figure 16 (MU-34601) shows typical results for the polarization in proton-proton scattering at 736 MeV as obtained with a polarized target.

When measuring polarization effects with a polarized target it is very advantageous to separate kinematically the scattering events on free hydrogen from the scattering on bound protons in the heavier nuclei of the target. Usually this kinematic separation is best obtained by counting both of the recoil particles after an elastic scattering. However we have made some attempts to isolate the scattering on free hydrogen by making measurements on only one particle in the final state. This has been important in pion-proton scattering at small angles, where the recoil proton does not get out of the polarized target. Figure 17 (MU-32813) shows a

differential range telescope that was used for counting low energy positive pions scattered from the polarized target. The scattered pions are incident from above. Those particles were counted which reached the counter R1 but did not reach the counter R2. The copper wedge was used to compensate for the change of pion energy with scattering angle. Figure 18 (MU-29815A) shows the resulting differential range curve from a polarized target and from a dummy target containing no hydrogen. One can see a small peak due to the scattering on free hydrogen, but the background is quite large so that it is hard by this method to get accurate measurements of the polarization in scattering.

When we came to measuring the polarization in pion-proton elastic scattering at higher energies we adopted the more elaborate apparatus shown in Fig. 19 (MUB-14036). Arrays of partially overlapping counters are used throughout this arrangement. The counters which define the scattering angle are called θ_{up} and θ_{down} depending upon which array they are part of. The counters labelled ϕ determine a coordinate in and out of the plane of the figure so that events could be separately detected depending upon whether they were coplanar with the beam or not. Figure 20 (MUB-14042) shows typical results for the polarization in elastic scattering of positive pions on protons for an incident momentum of 1.352 GeV/c. Figure 21 (MUB-14049) shows the corresponding results at 2.912 GeV/c. Notice that we were able to cover only a portion of the range of scattering angles. This is mostly due to the fact that where the cross section got very small it was difficult to get enough counts to give a significant result.

For the elastic scattering of spin 0 particles on spin 1/2 particles, such as for elastic pion-proton scattering, the scattering matrix is rather simple:

$$M = f(\theta) + i\, g(\theta)\, \vec{\sigma} \cdot \vec{n}$$

The terms f and g are complex numbers, functions of the energy and angle of scattering. It is well known that where the ratio of g to f takes on the value +i, the polarization should be 100%. It has been pointed out to me by Dr. Gilbert Shapiro, one of my colleagues at Berkeley, that in varying the energy and angle of scattering, one should expect occasional cases which give this 100% polarization in scattering. Alternatively, when g/f is -i,

the polarization should be -100%. Figure 22 shows that around the region of 100% polarization there is a sizeable region in the g/f diagram in which the polarization is surprisingly close to 100%. During the next year we hope to explore some of these regions where the polarization is very high, with the hope of establishing definite energies and scattering angles at which the polarization in pion-proton scattering passes through 100%, as a means of identifying situations that can be used to check the measurements of the target polarization. We are generally quite trustful of the basic method of measuring target polarization, but since the beams that we use rarely irradiate the target quite uniformly over its total volume, we are always in doubt that the average polarization seen by the measuring apparatus and the average polarization seen by the beam are exactly the same. If these special angle and energies could be established that gave 100% polarization in scattering, we could use these situations to measure target polarization, perhaps more accurately than we are now able to.

In recent years we have collaborated with other experimentalists at the Stanford Linear Accelerator Center (SLAC), to study electron scattering from polarized protons in a polarized proton target. In particular, it was possible that the inelastic electron scattering on polarized protons could show some demonstration of the failure of time reversal invariance. The experimental arrangement is shown in Fig. 23 (XBL6911-6279). The figure is not drawn to scale; it is purely schematic. Beam monitoring was accomplished by Toroid 1, Toroid 0, and a secondary emission quantometer at the beam dump. Because it was necessary to use a rather high intensity electron beam, provision was made for vertical and horizontal deflection coils that could sweep the beam across the polarized target in a manner reminiscent of the beam sweep in a television cathode ray tube. It was also necessary to use a polarized target made of butanol because butanol is least susceptible to radiation damage among the known polarized target materials. Figure 24 (XBL702-2353) shows the set-up near the polarized target. Figure 25 (XBL708-1773) shows the raster pattern or sweep pattern of the beam across the polarized target. To improve the resolution of the magnetic spectrometers that detected the scattered electrons, the polarized target was divided, for counting purposes, into three segments: the top third, the

middle third, and the bottom third. Figure 25 shows the transition points between the different segments of the polarized target.

In spite of the precautions taken to minimize radiation damage on the polarized target, the polarization decreased appreciably in just a few hours running. Figure 26 (XBL702-2355) shows the pattern of decreasing polarization with increasing beam dose. The vertical discontinuities represent occasions on which the polarized target was annealed by bringing up the temperature to -40°C, where there is a phase transition in butanol. After annealing, the target could be used for a few hours more. Nevertheless, the target material had to be completely replaced about once each day of running. Figure 26 shows the data for a beam of gamma rays, but the results for an electron beam are very similar.

In the electron scattering experiments with an incident electron of known energy, the mass of the recoiling hadronic system could be calculated from the observed energy and angle of the scattered electron. In this calculation it was necessary to assume that the scattering occurred on a free proton. In fact, there is much scattering on bound protons in the heavier elements of the polarized target, so the observed events were not all due to the free protons that were polarized. To interpret the results of this experiment, it was necessary to know what fraction of the counts were due to polarized protons in the target. Figure 27 (XBL706-3216) shows the observed counting rates for the actual alcohol polarized target and for a carbon target, as well as the calculated fraction of the observed counts that came from free hydrogen, as functions of the missing mass, namely, the mass of the unobserved recoiling hadrons. Of course, the effective target polarization was greatly reduced by the fact that we had to include in our counts many counts from scattering on bound protons.

Because the final asymmetries in the electron scattering experiments were expected to be very small, it was important to eliminate small systematic errors which might lead to a false result. To aid in looking for errors, particularly random errors that were not apparent to the casual observer, we re-did the calculation of the results for a number of pretended patterns of time dependence of the polarization. Figure 28 (XBL708-1770) shows some of these patterns in time that we called test asymmetries. At the top of

the figure is shown the real dependence of the polarization on time, namely the time pattern with which the target was polarized positively and negatively. As an aid in assessing random errors, we also calculated results that we called test results based on hypothetical patterns of polarization shown on the lines below. Some of these test patterns included changes of sign of the hypothetical polarization with the same period as the actual polarization changed. Other patterns used longer periods or shorter periods than the actual polarization pattern. Each of the computed test asymmetries should be zero within experimental error, but the use of many test asymmetries allowed a better evaluation of the extent of random errors in the data. With the use of several beam energies, several portions of the polarized target (upper one-third, middle one-third, and lower one-third), various bins of missing mass, and a large number of different test asymmetry patterns, we were able to obtain very good statistics on the random errors. Figure 29 (XBL706-3210) shows the number of times there were deviations of various numbers times the calculated standard deviation. The agreement of the points with the theoretical curve indicates that the random errors were very well given by the calculated statistical errors, within about three percent.

Figure 30 (XBL706-1081) shows the results for elastic electron-proton scattering as a function of the invariant four-momentum transfer squared. These results are consistent with zero asymmetry, suggesting that any possible two-photon exchange diagrams are not important in this scattering process.

Figure 31 (XBL708-1712) shows the observed asymmetries for the inelastic scattering of electrons and positrons on polarized protons, calculated as they would appear if the polarized target were in fact 100% polarized. We believe that all these results are consistent with zero, indicating there is no evidence in this process for any failure of time reversal invariance.

Figure 32 (XBL702-2356) shows the results we were able to obtain on the asymmetry in pion photoproduction on polarized protons. It was possible to do this experiment in the same physical set-up as was used for the electron scattering on polarized protons.

I will close this lecture by mentioning one item of current business in Berkeley, namely the construction of some super-conducting coils to provide the main magnetic field for the polarized target. The purpose of constructing super-conducting coils is to allow doing the experiments of different kinds than can be done with the existing iron magnets. In the existing magnets, it is nearly impossible to observe particles that are scattered in the direction of the pole pieces of the magnet. Thus, we are in practice restricted to cases in which the target polarization is perpendicular to the scattering plane. By constructing super-conducting coils, we hope to open up our range of experimental capabilities to include cases in which the target is polarized in a direction in the scattering plane. Figure 33 (XBL726-1240) shows a partial cross section diagram of proposed super-conducting coils. The coils turn around the indicated axis of rotation, being in each case pairs of coils in Helmholtz geometry. The other pair of coils in each case to make up the Helmholtz geometry is not shown, being symmetrically located with respect to the indicated plane of symmetry. In our design the main coil consists of four elements of about equal size. Closer to the center of the arrangement is a small correcting coil, also part of a set of Helmholtz coils. The small correcting coil works with reverse current to lessen some of the inhomogeneities that remain even with a Helmholtz coil configuration. At the present time there is doubt about whether these colls will actually be built in the form shown, because they turn out to be very expensive. For an arrangement in which the average radius of the main coil is about 30 cm., the estimated cost is sixty-million yen. We will be studying alternatives to see if the cost can be brought down. While at present the cost seems prohibitive, we calculate that these coils, if constructed, would give a very satisfactory field. For a model in which the radius of the main coil was 25 cm on average, the region in which the field was accurate to four parts in 10^4 included a sphere of radius 5 cm, quite adequate for a useful polarized target. Therefore, we hope to find some less expensive way of achieving a magnetic field almost as good. If we had these super-conducting coils, we could do some of the determinations of the Wolfenstein parameters called R and A. We believe that these measurements can be quite important in many nuclear

scattering processes, including pion-nucleon scattering. In fact, if I look ahead to the years when the new accelerator at Tsukuba will be operating, I believe I could predict that these measurements of the parameters R and A may be quite important to be done within your new laboratory.

Thank you.

REFERENCES

[1] Lincoln Wolfenstein, Annual Review of Nuclear Science, Vol. 6, p. 43, 1956.

[2] Carson D. Jeffries, Dynamic Nuclear Orientation, Interscience Publishers, New York, 1963.

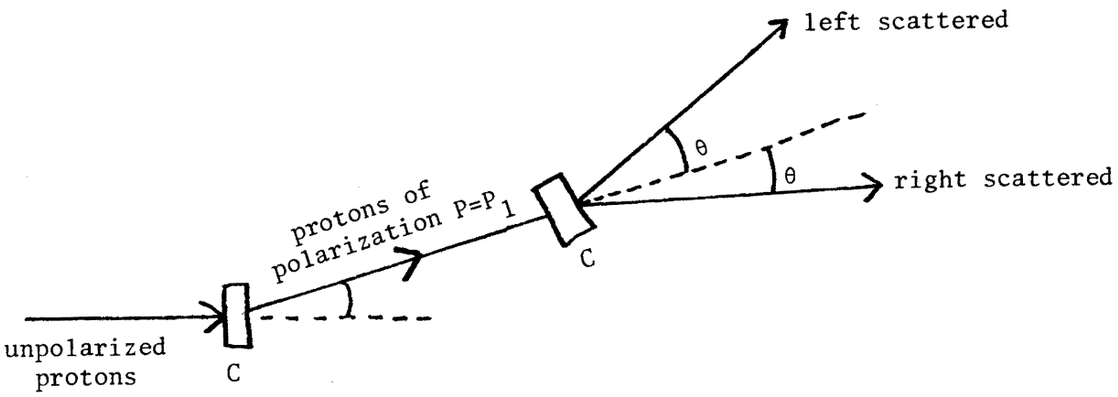
left scattered
θ
θ
right scattered
protons of
polarization P=P1
C
unpolarized
protons
C

Fig. 1

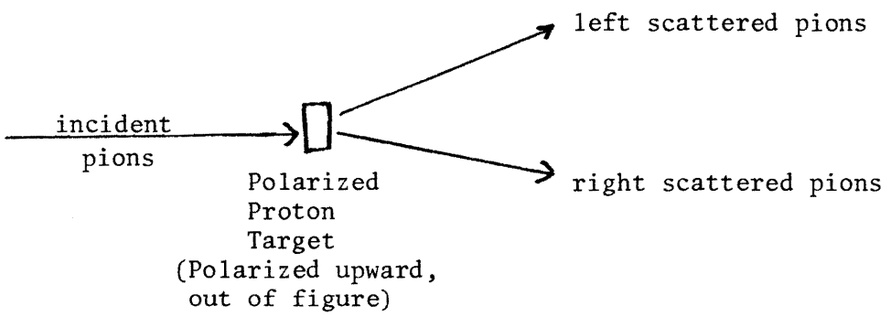
left scattered pions
incident
pions
right scattered pions
Polarized
Proton
Target
(Polarized upward,
out of figure)

Fig. 2

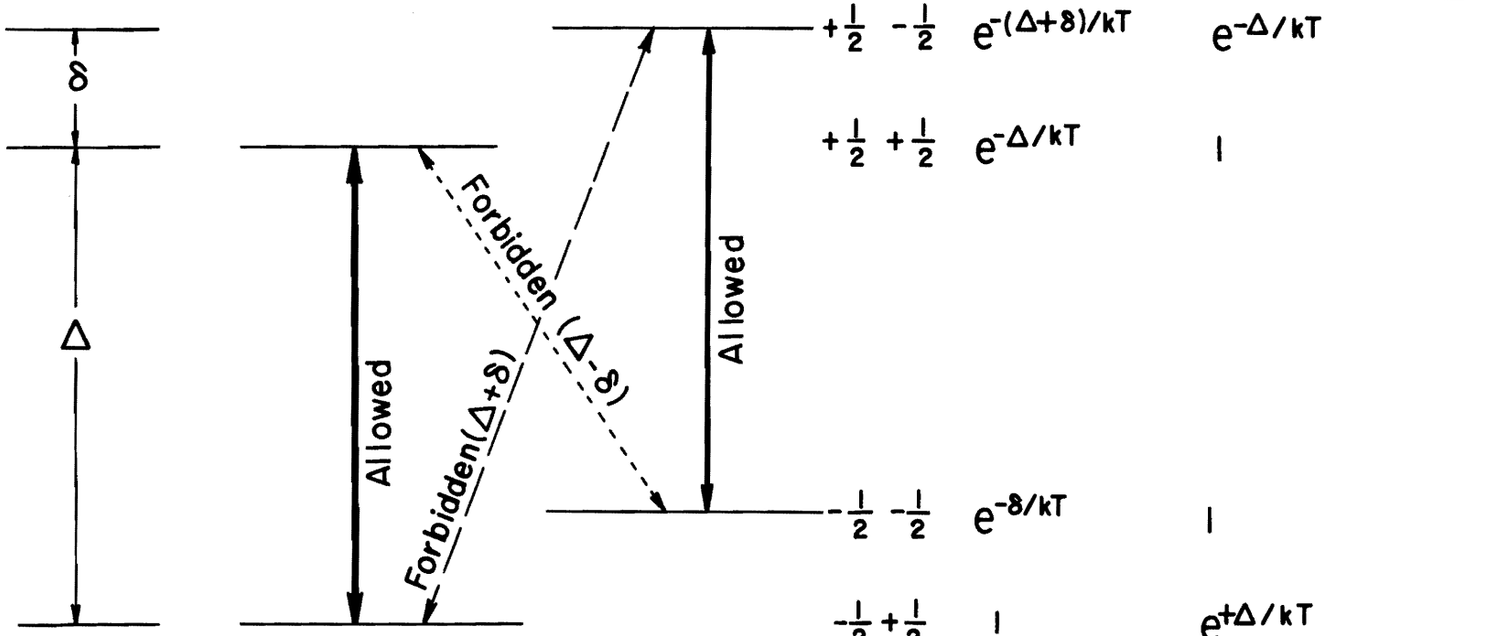
δ
Δ
Allowed
Forbidden (Δ-δ)
Forbidden (Δ+δ)
Allowed
M m
Relative population at thermal equilibrium
Relative population when saturating Δ - δ
+½ -½ e^-(Δ+δ)/kT e^-Δ/kT
+½ +½ e^-Δ/kT 1
-½ -½ e^-δ/kT 1
-½ +½ 1 e^+Δ/kT

MU-32843

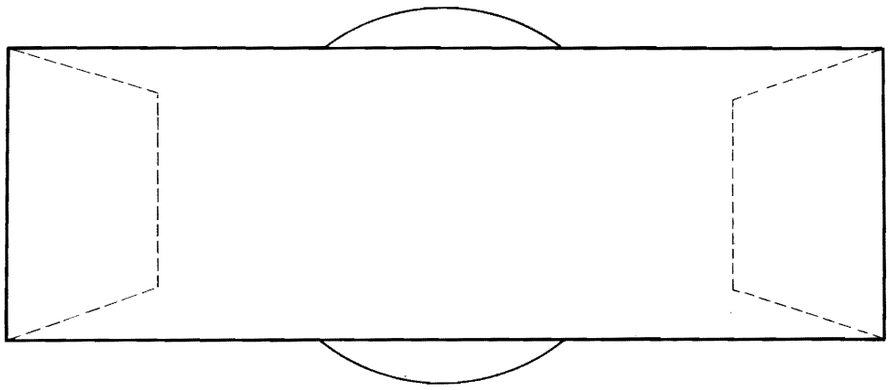

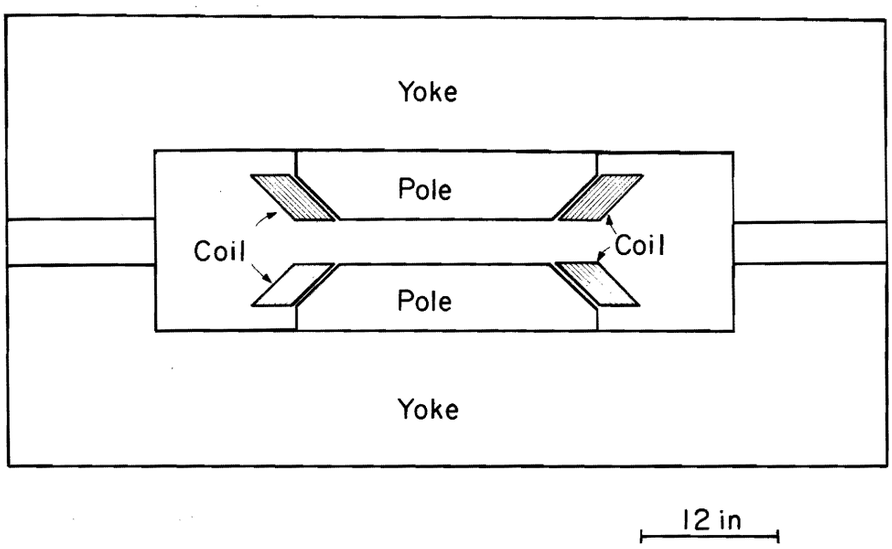

MUB-2238

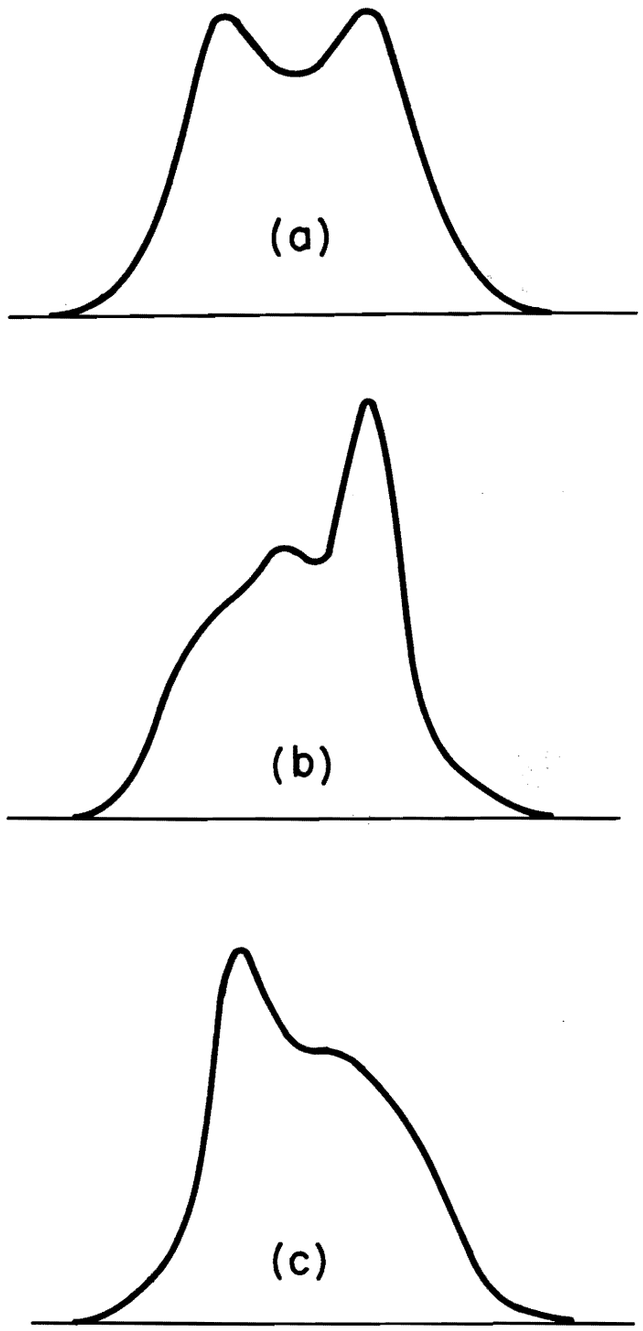

MU-32816

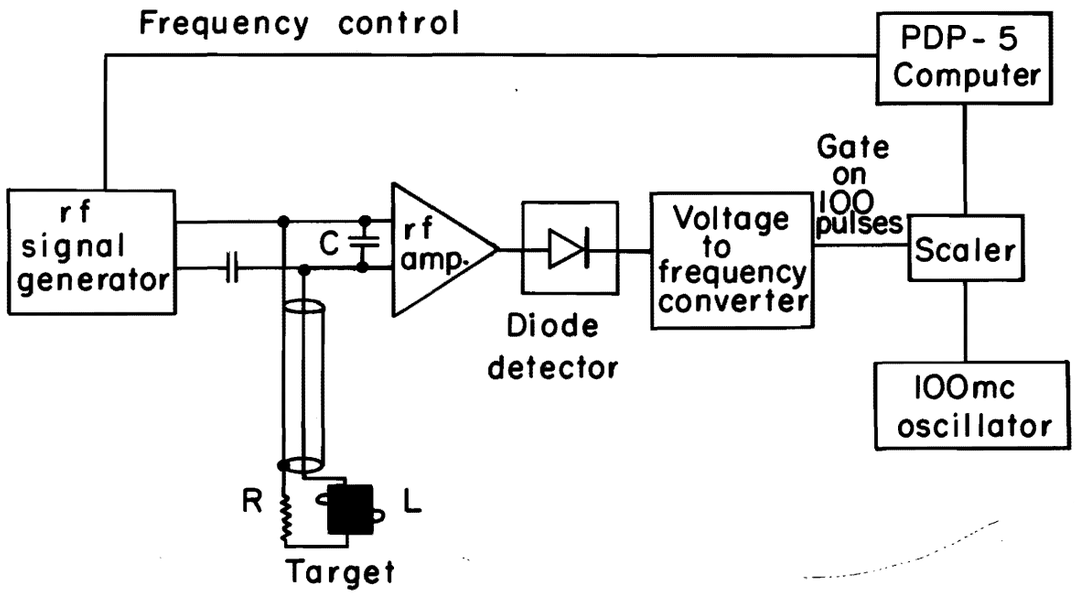
Frequency control
PDP-5 Computer
rf signal generator
C
rf amp.
Diode detector
Voltage to frequency converter
Gate on 100 pulses
Scaler
100mc oscillator
R
L
Target

XBL707-3434

Proton NMR Signal
Showing Background Subtraction Sequence

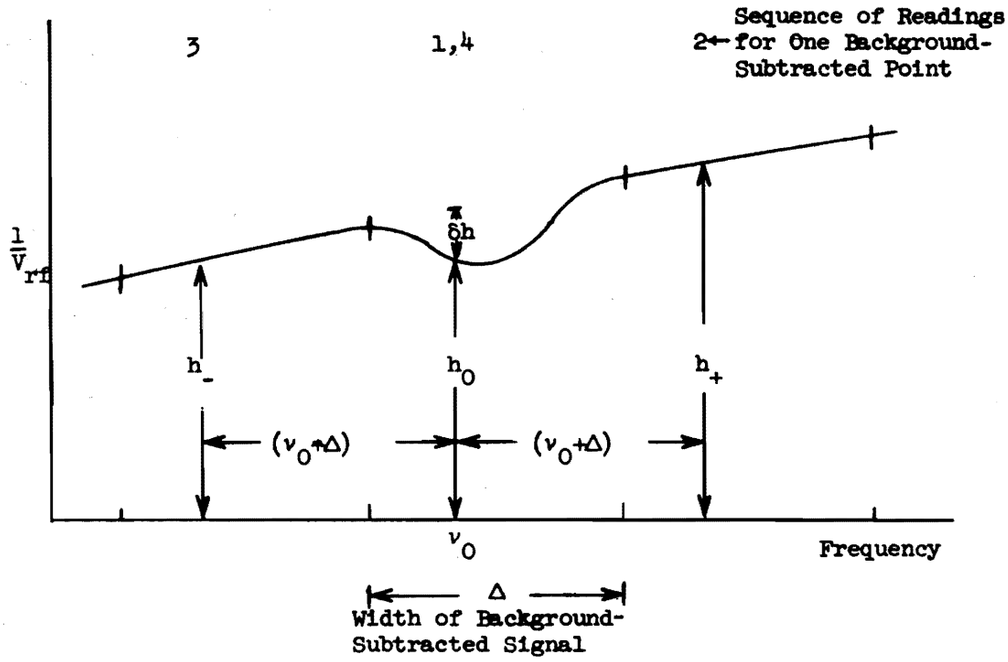

Background-Subtracted Signal
Displayed on PDP-5 Oscilloscope

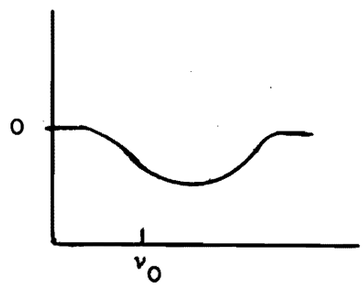

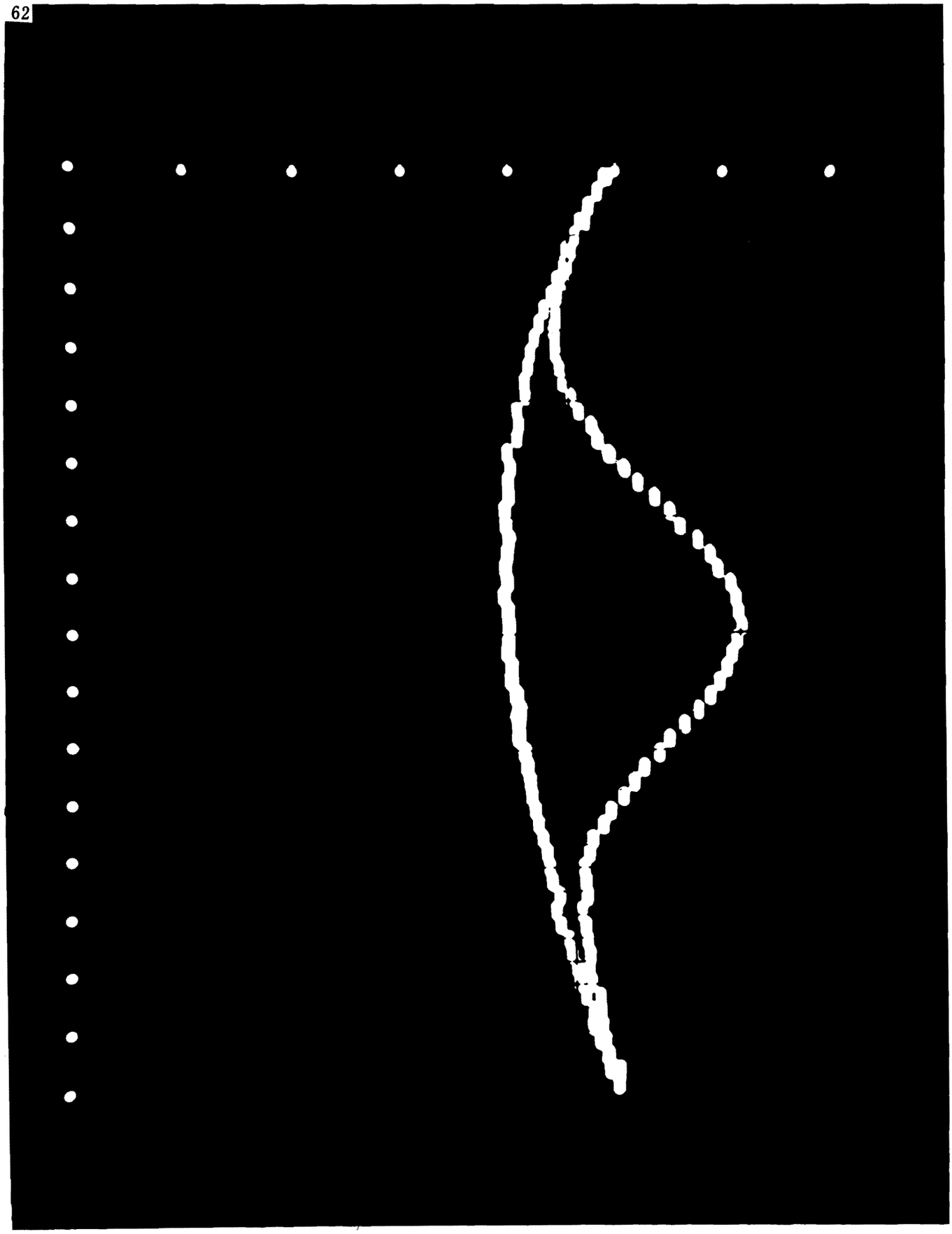

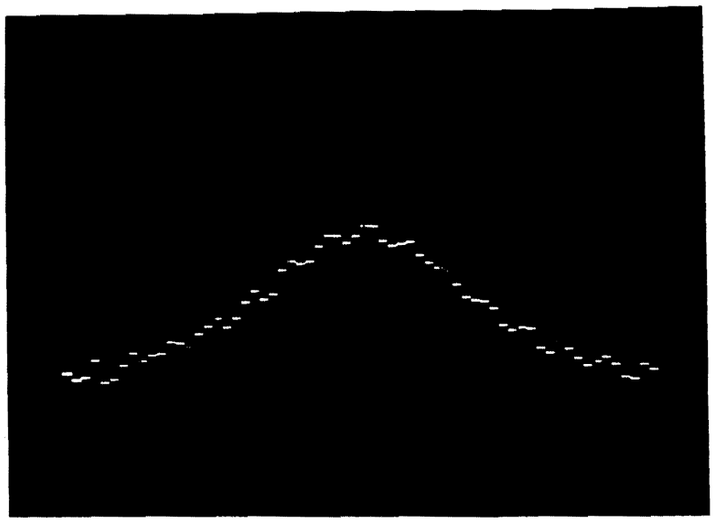

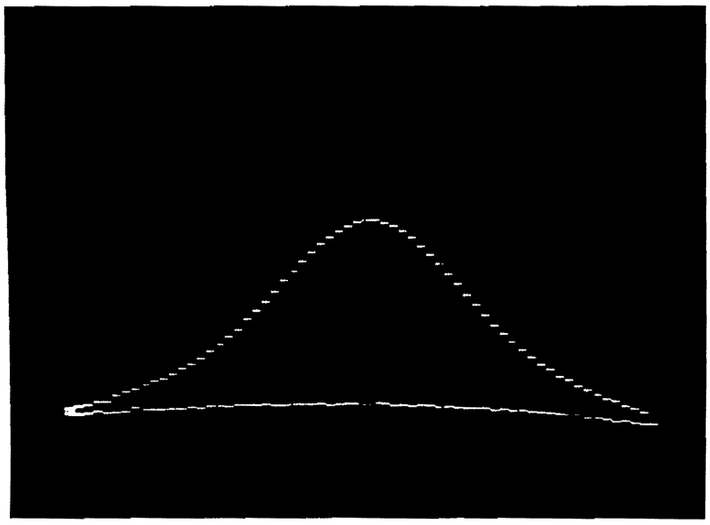

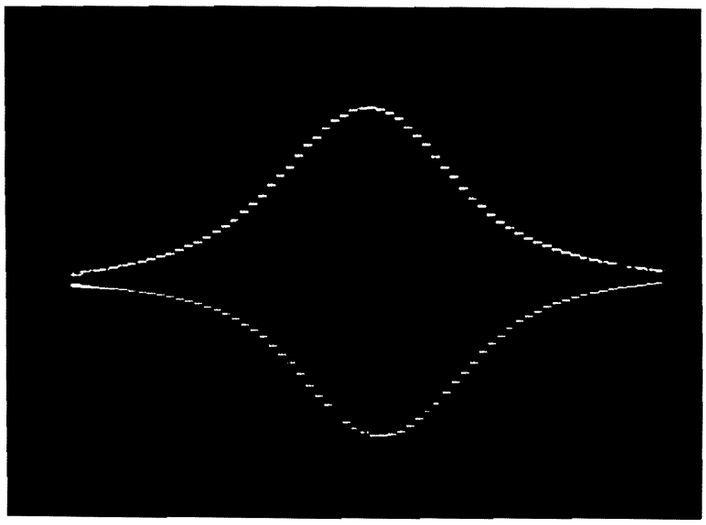

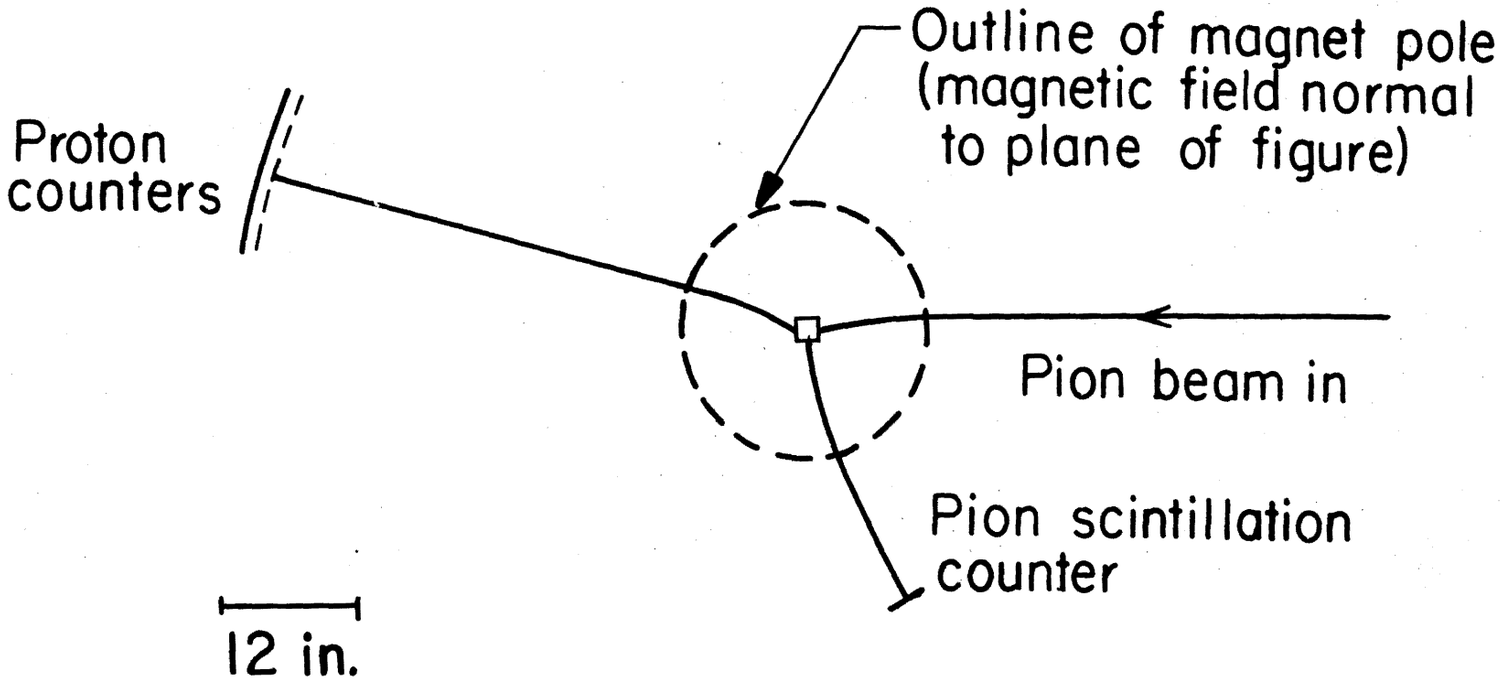
Outline of magnet pole
(magnetic field normal
to plane of figure)
Proton
counters
Pion beam in
Pion scintillation
counter
12 in.

MU-30598A

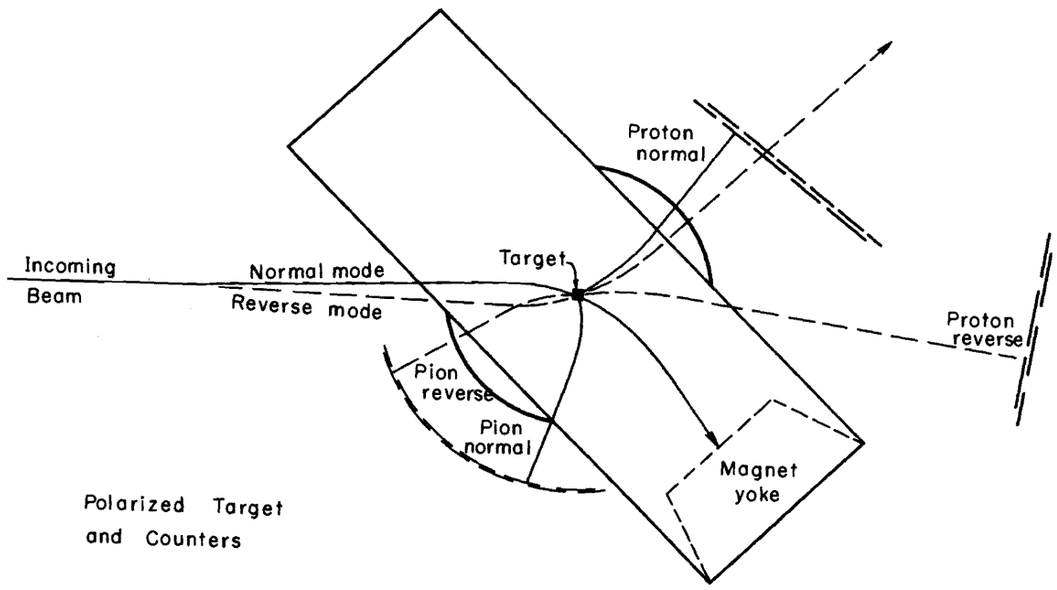
Proton
normal
Incoming
Beam
Normal mode
Reverse mode
Target
Proton
reverse
Pion
reverse
Pion
normal
Magnet
yoke
Polarized Target
and Counters

MUB-10360

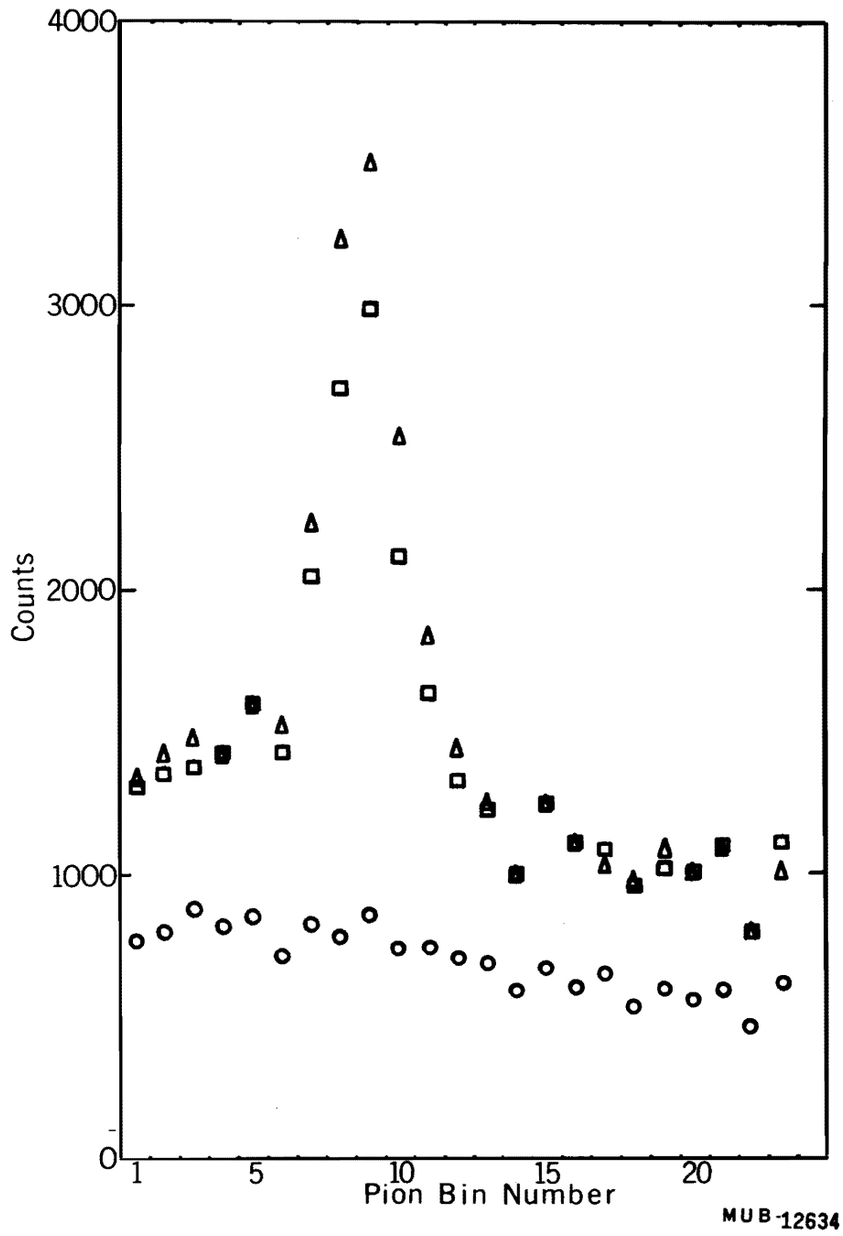
4000
3000
2000
1000
0
Counts
1
5
10
15
20
Pion Bin Number
MUB-12634

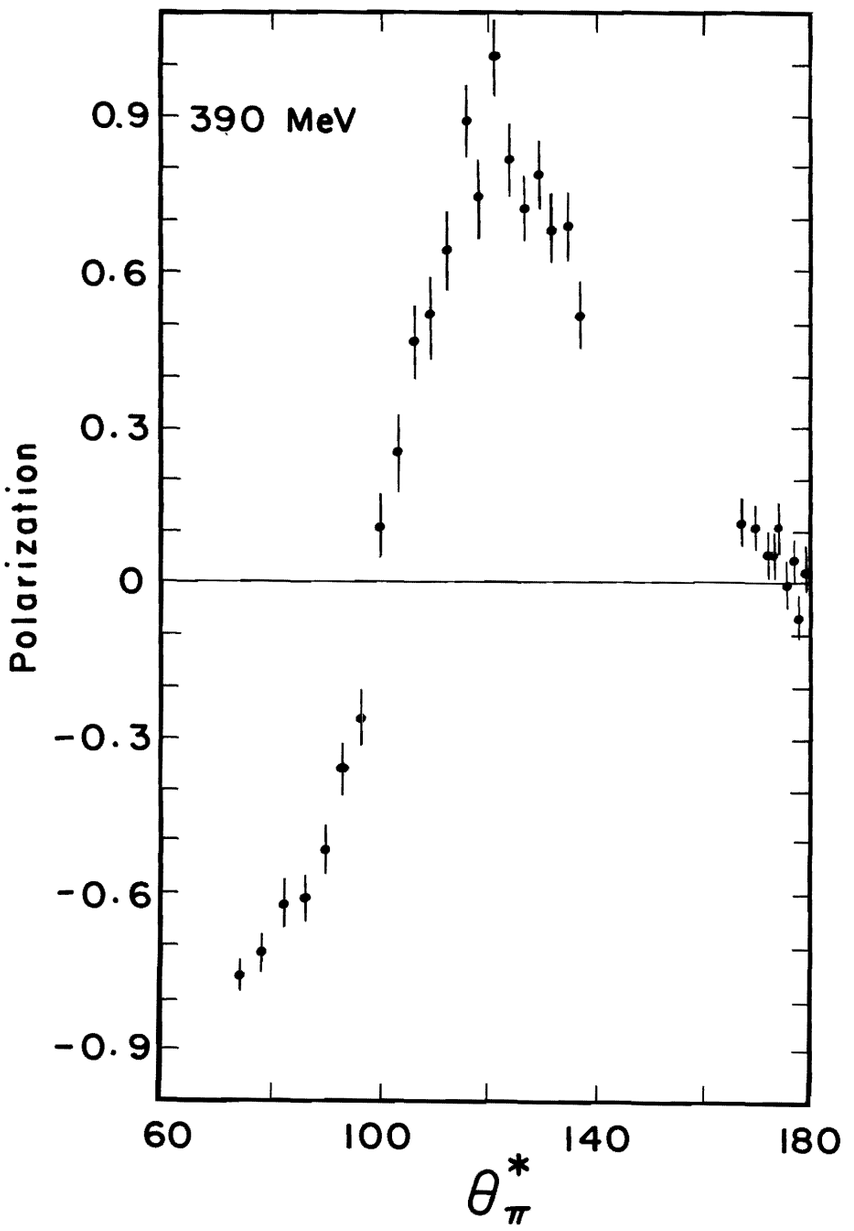
390 MeV
0.9
0.6
0.3
0
-0.3
-0.6
-0.9
Polarization
60
100
140
180
θ_π^*
MUB-12294

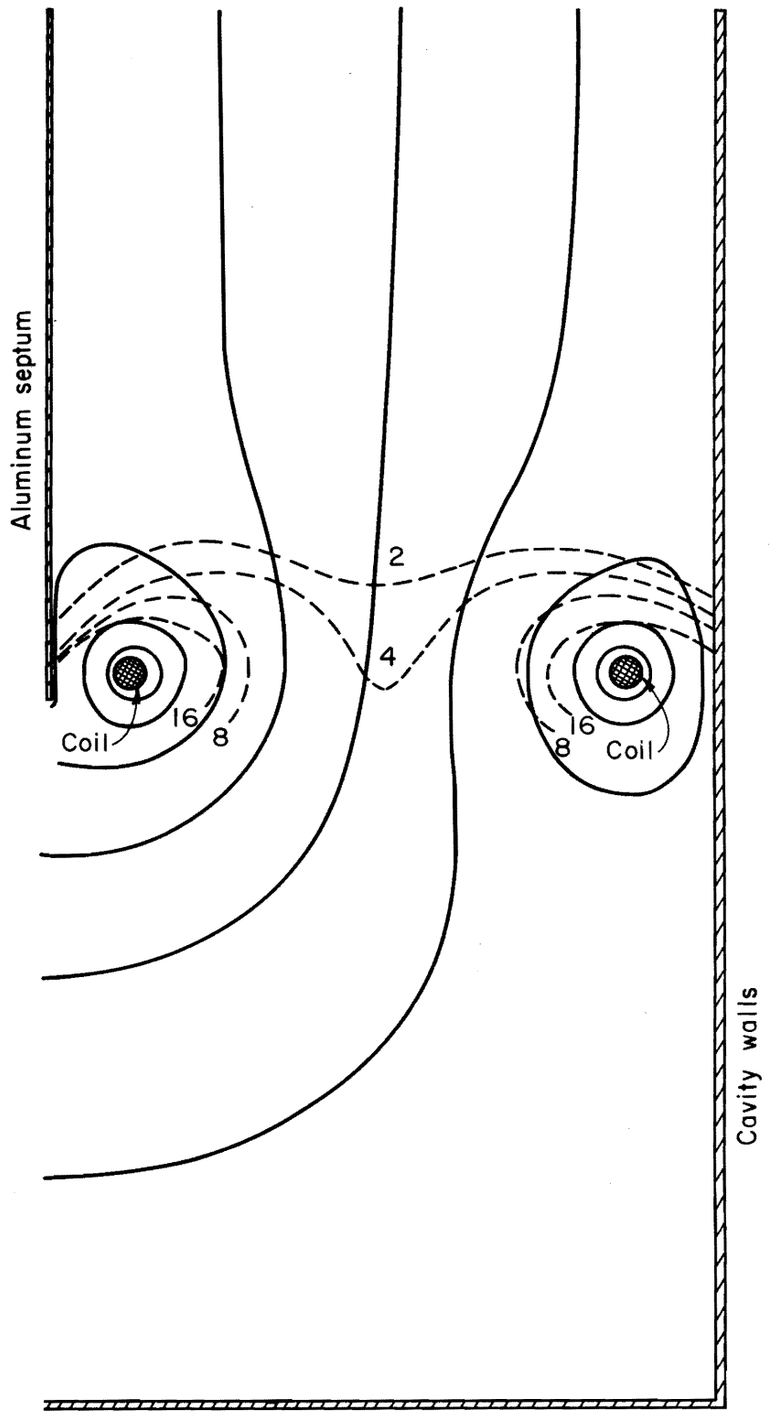

MU-34597

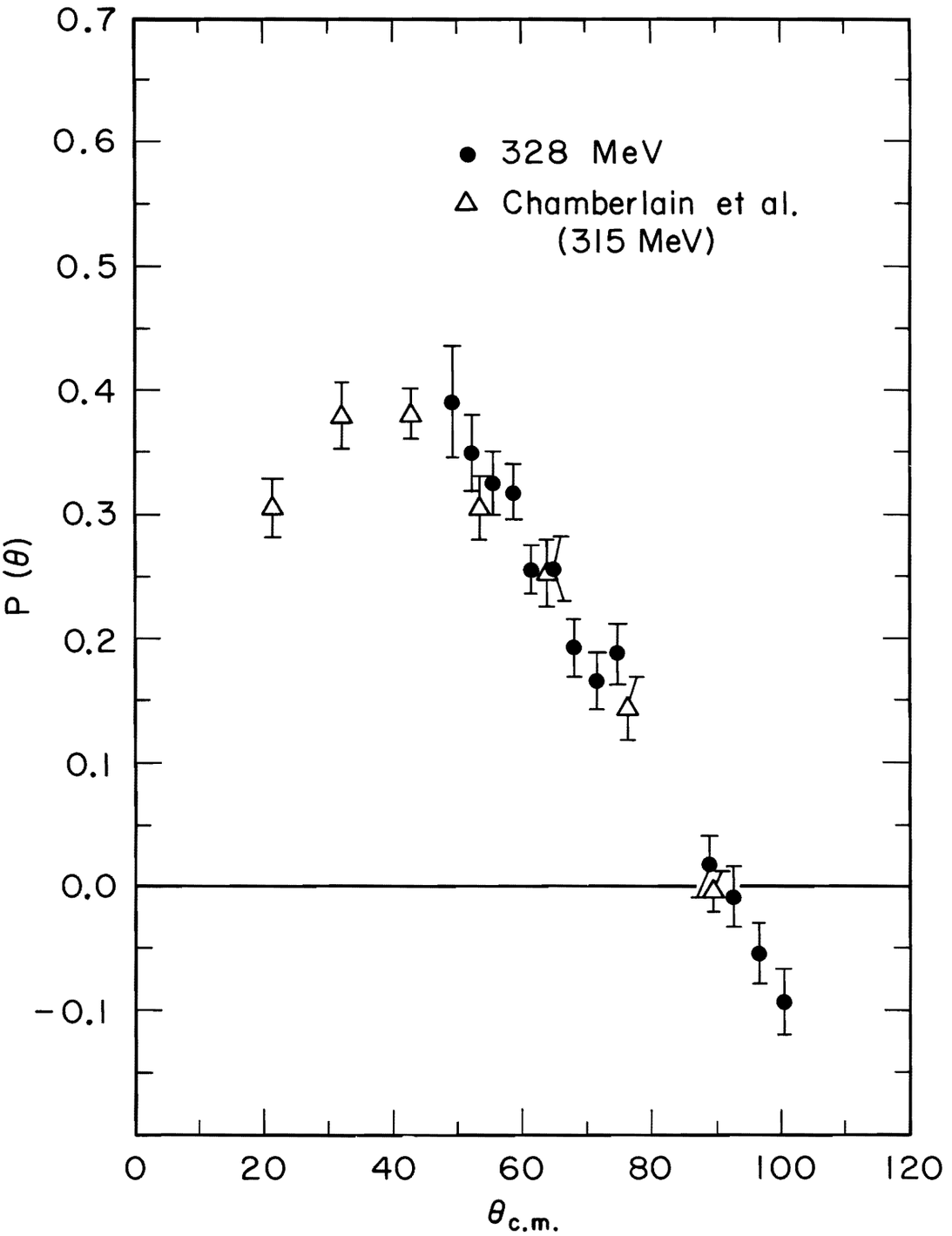
0.7
0.6
0.5
0.4
0.3
0.2
0.1
0.0
−0.1
P (θ)
● 328 MeV
△ Chamberlain et al.
(315 MeV)
0
20
40
60
80
100
120
θc.m.

MU-34598

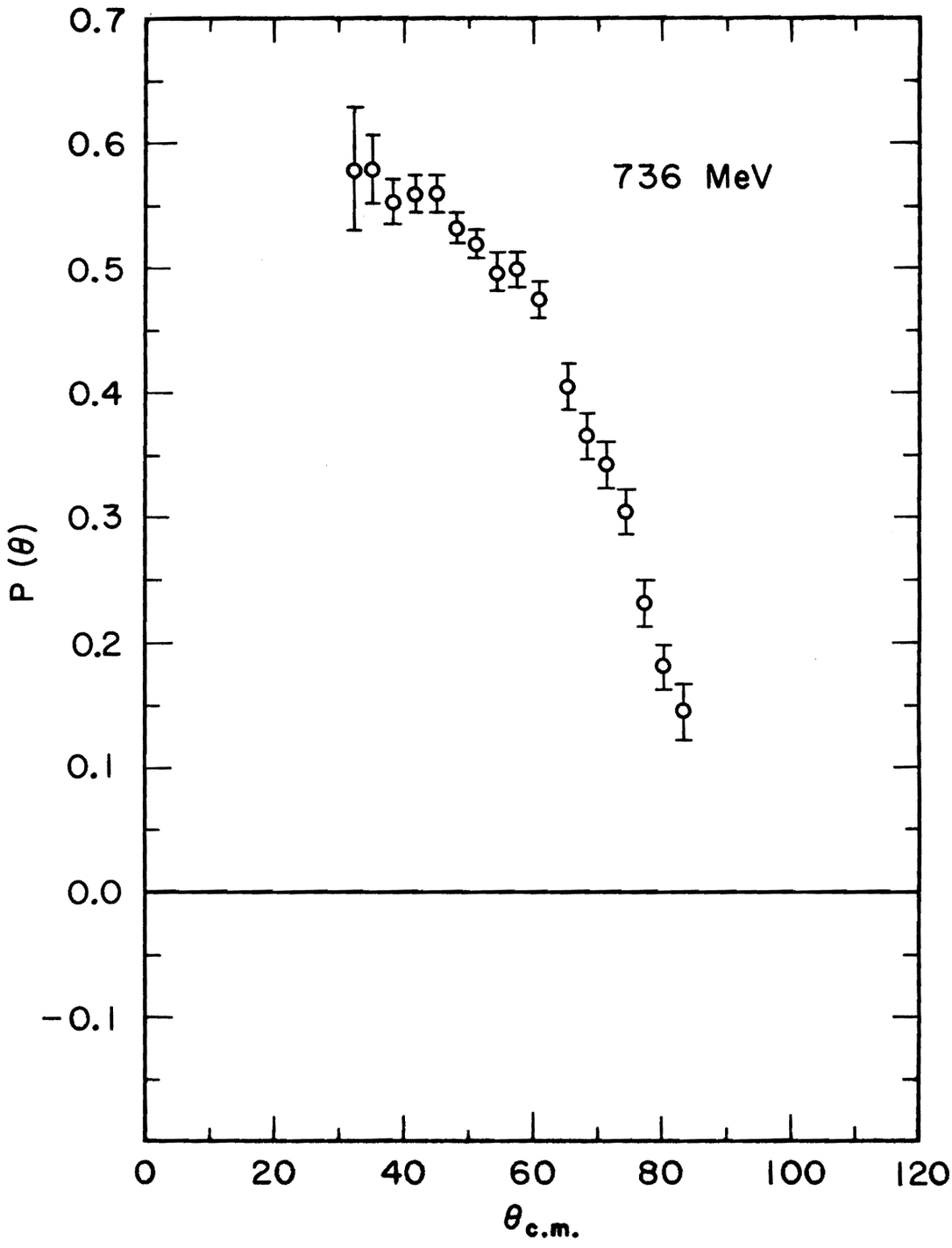

MU-34601

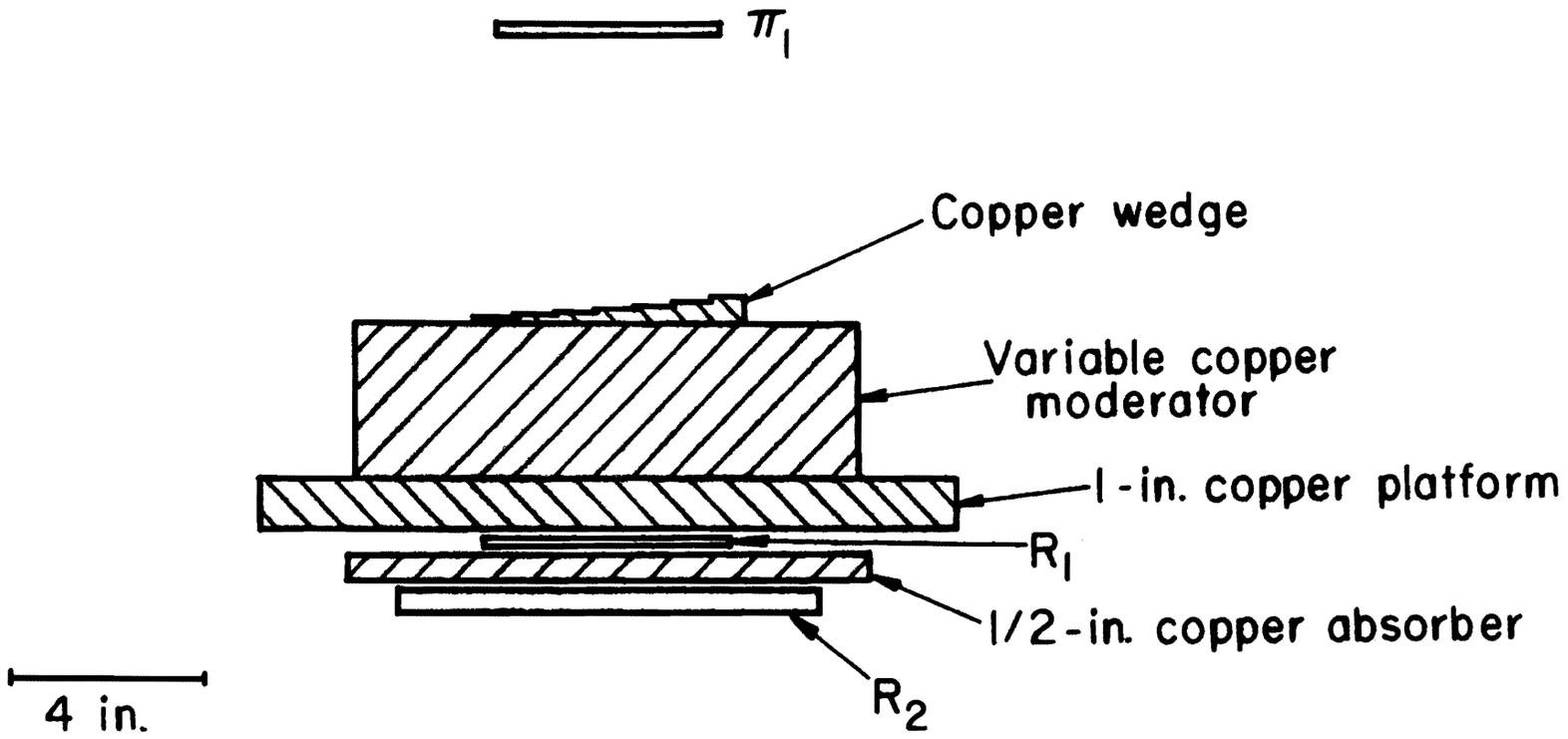
π_1
Copper wedge
Variable copper moderator
1-in. copper platform
R_1
1/2-in. copper absorber
R_2
4 in.

MU-32813

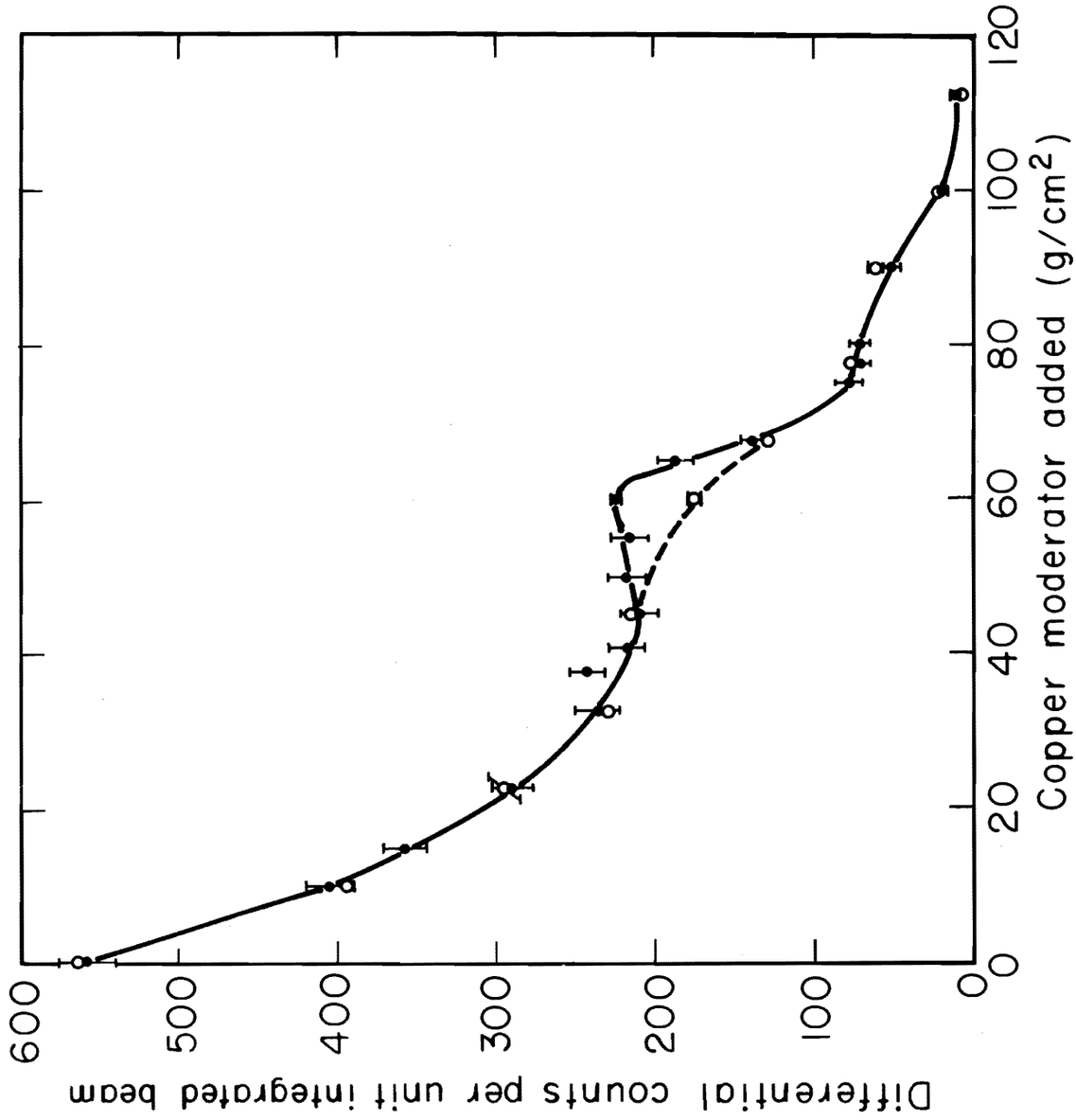
Differential counts per unit integrated beam
600
500
400
300
200
100
0
0
20
40
60
80
100
120
Copper moderator added (g/cm²)

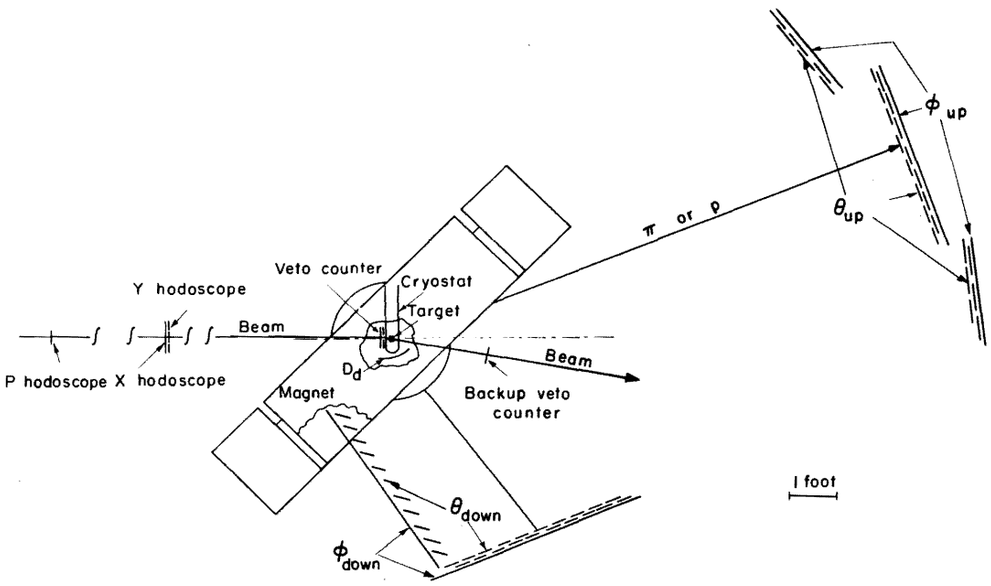

Experimental arrangement

MUB-14036

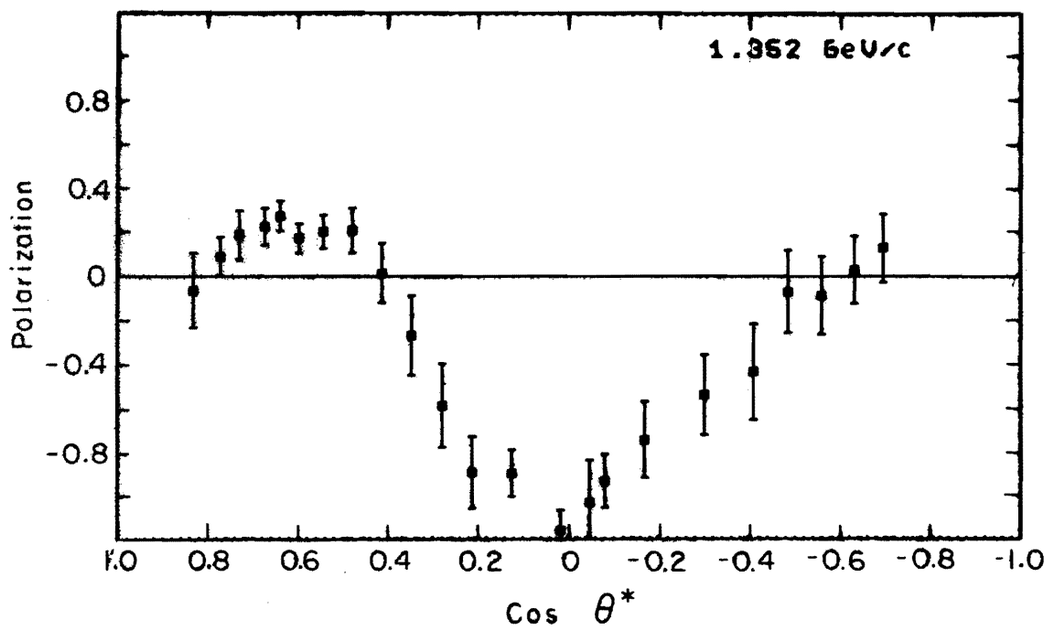
1.362 GeV/c
Polarization
0.8
0.4
0
-0.4
-0.8
1.0
0.8
0.6
0.4
0.2
0
-0.2
-0.4
-0.6
-0.8
-1.0
Cos θ*

MUB 14042

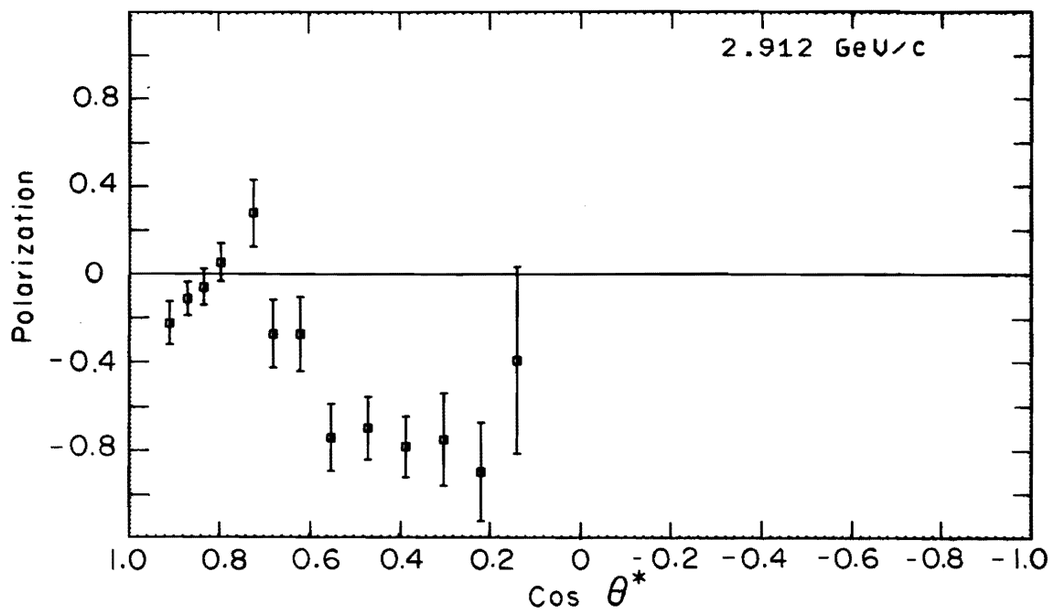
2.912 GeV/c
Polarization
0.8
0.4
0
-0.4
-0.8
1.0
0.8
0.6
0.4
0.2
0
-0.2
-0.4
-0.6
-0.8
-1.0
Cos θ*

MUB-14049

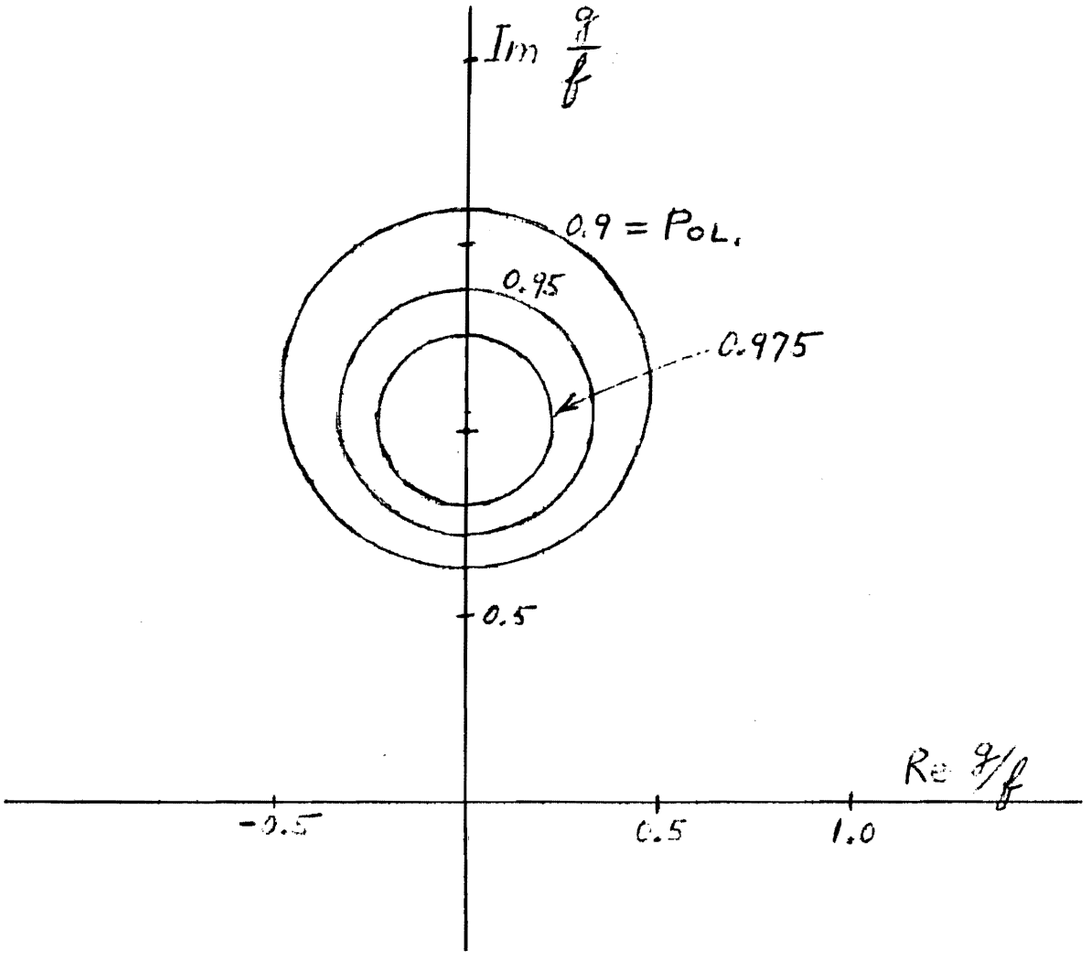
Im q/f
0.9 = POL.
0.95
0.975
0.5
Re q/f
-0.5
0.5
1.0

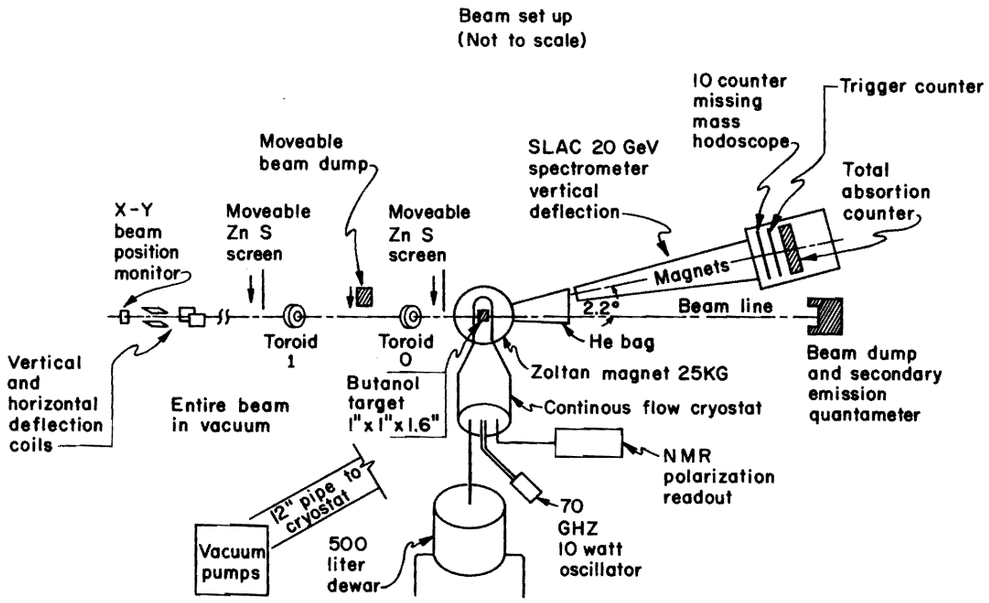

XBL6911-6279

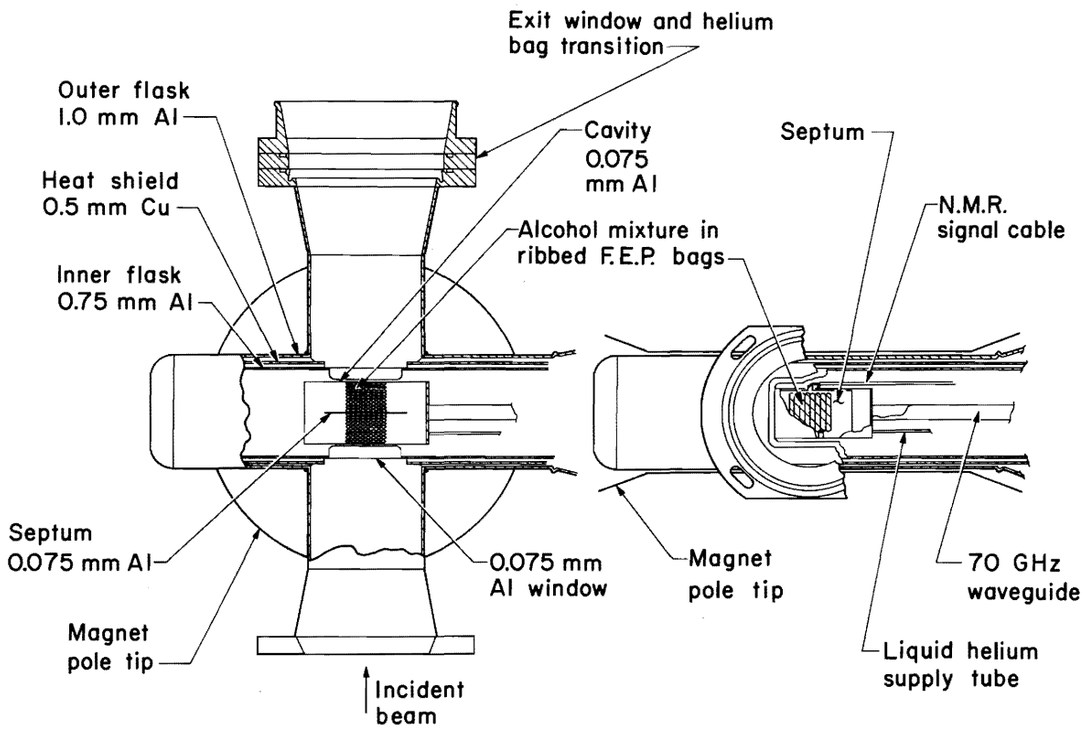
Exit window and helium
bag transition
Outer flask
1.0 mm Al
Cavity
0.075
mm Al
Septum
Heat shield
0.5 mm Cu
N.M.R.
signal cable
Alcohol mixture in
ribbed F.E.P. bags
Inner flask
0.75 mm Al
Septum
0.075 mm Al
0.075 mm
Al window
Magnet
pole tip
Magnet
pole tip
70 GHz
waveguide
Liquid helium
supply tube
Incident
beam
(a)
(b)

XBL702-2353

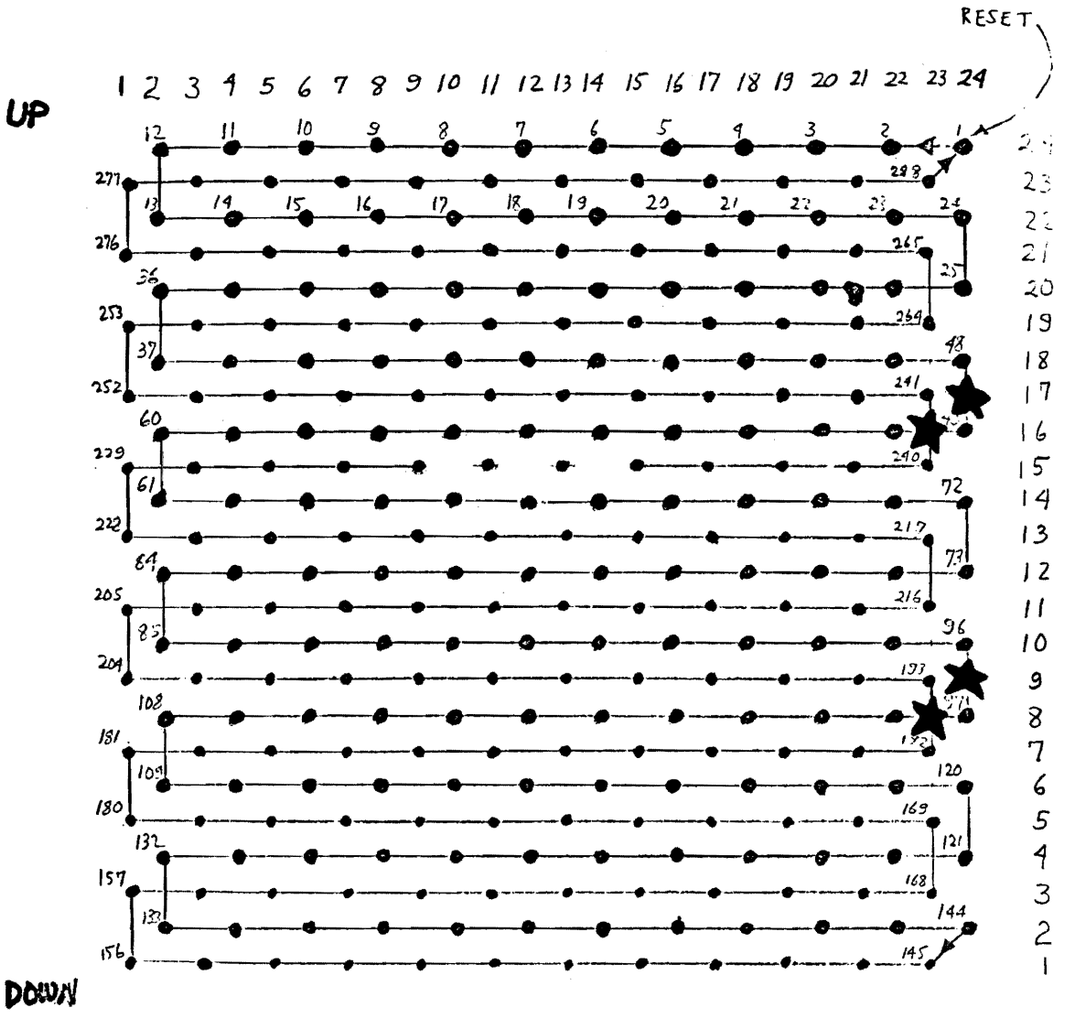

"The Raster"

XBL 708-1773

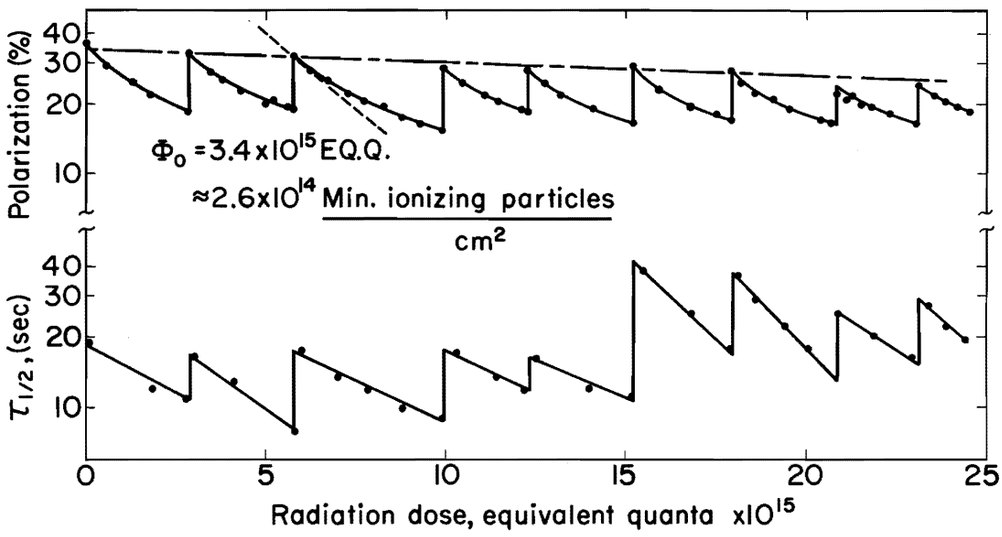
Polarization (%)
40
30
20
10
$\Phi_0 = 3.4 \times 10^{15}$ EQ.Q.
$\approx 2.6 \times 10^{14}$ Min. ionizing particles / cm^2
$\tau_{1/2}$, (sec)
40
30
20
10
0
5
10
15
20
25
Radiation dose, equivalent quanta x10^{15}

XBL702-2355

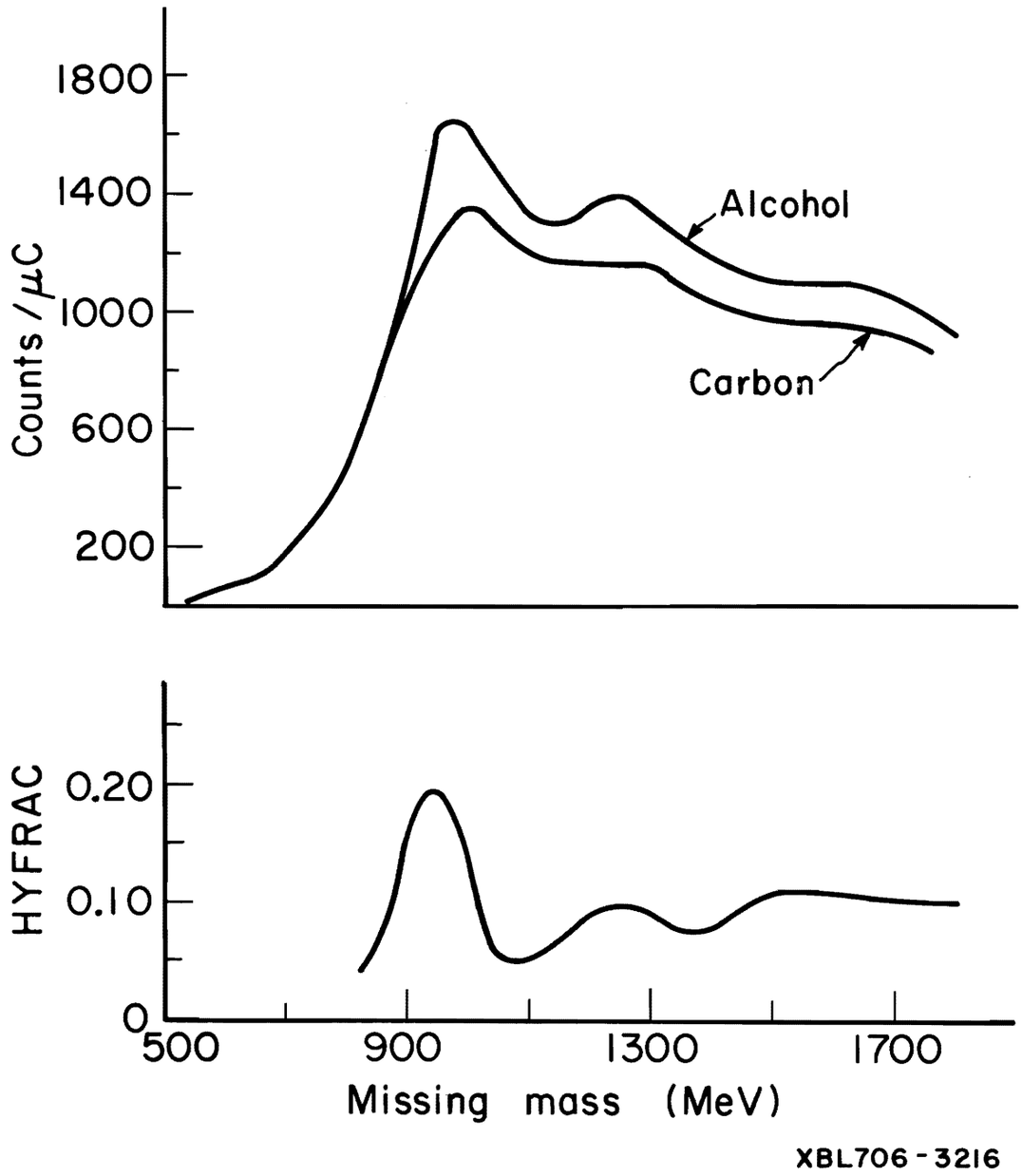
1800
1400
1000
600
200
Counts / μC
Alcohol
Carbon
0.20
0.10
0
HYFRAC
500
900
1300
1700
Missing mass (MeV)

XBL706-3216

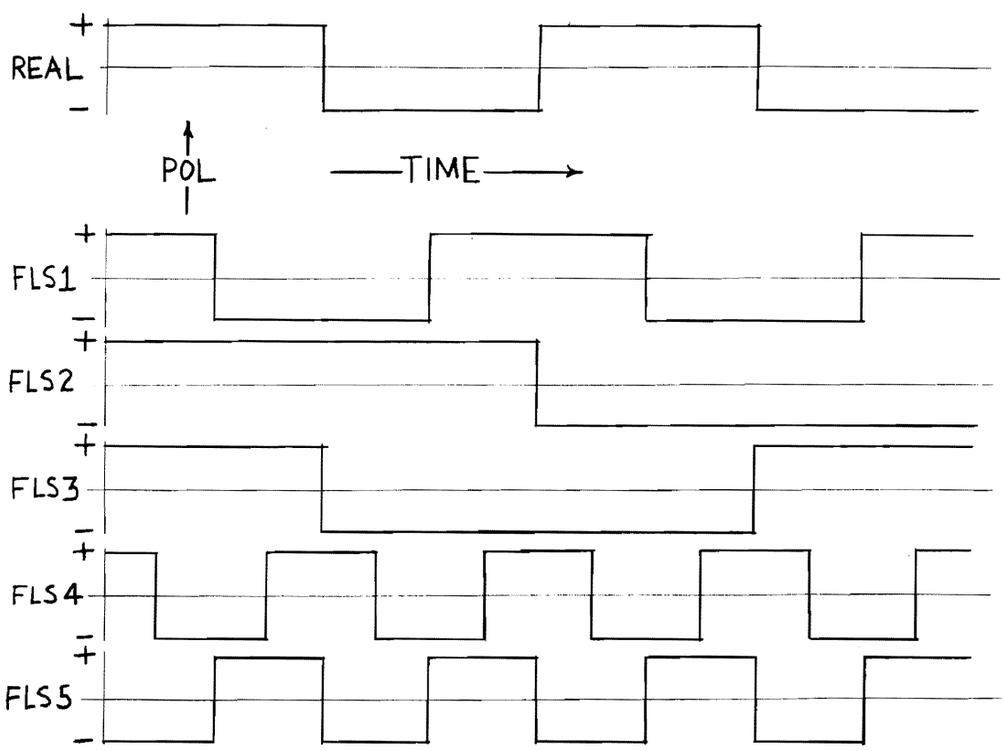

XBL 708-1770

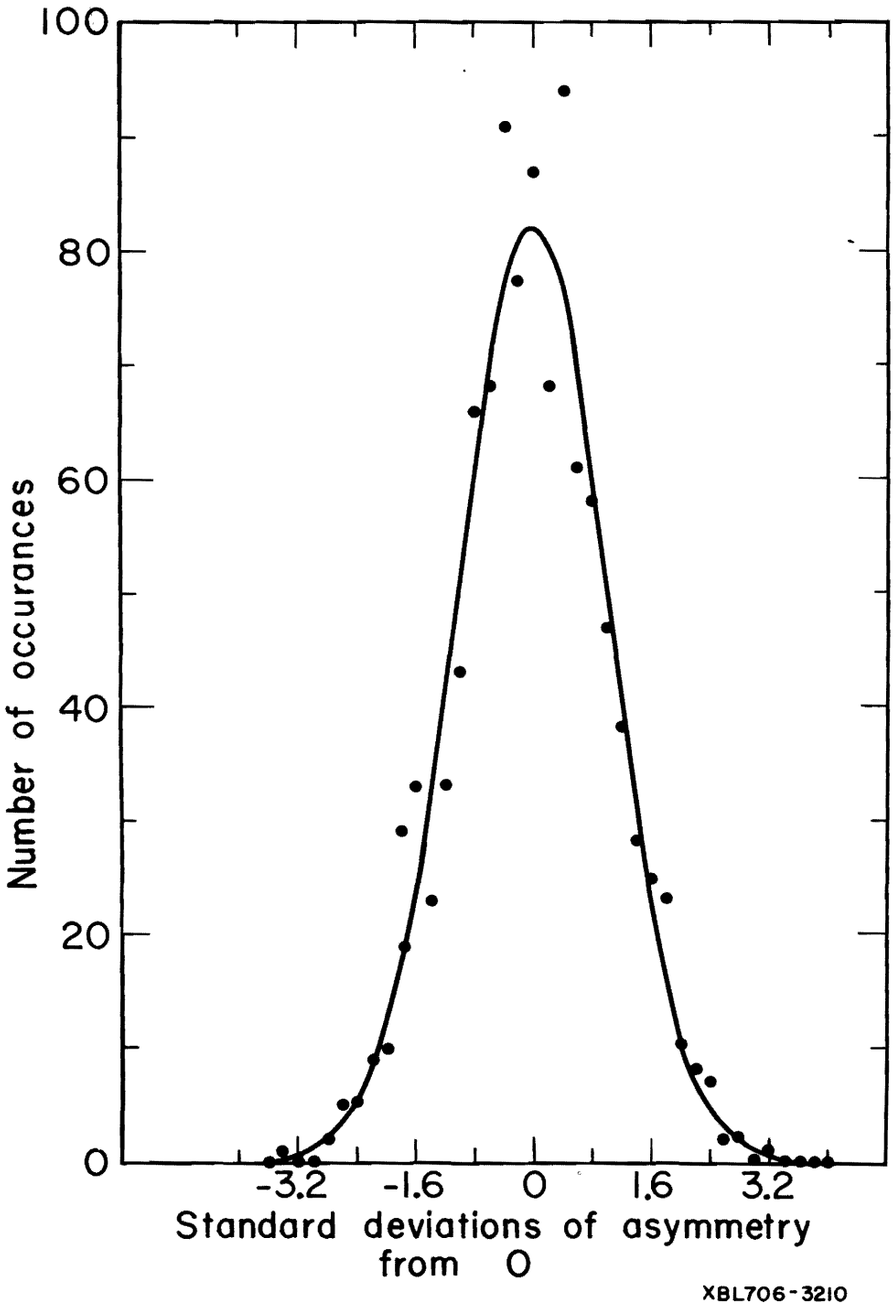
100
80
60
40
20
0
Number of occurances
-3.2
-1.6
0
1.6
3.2
Standard deviations of asymmetry
from 0
XBL706-3210

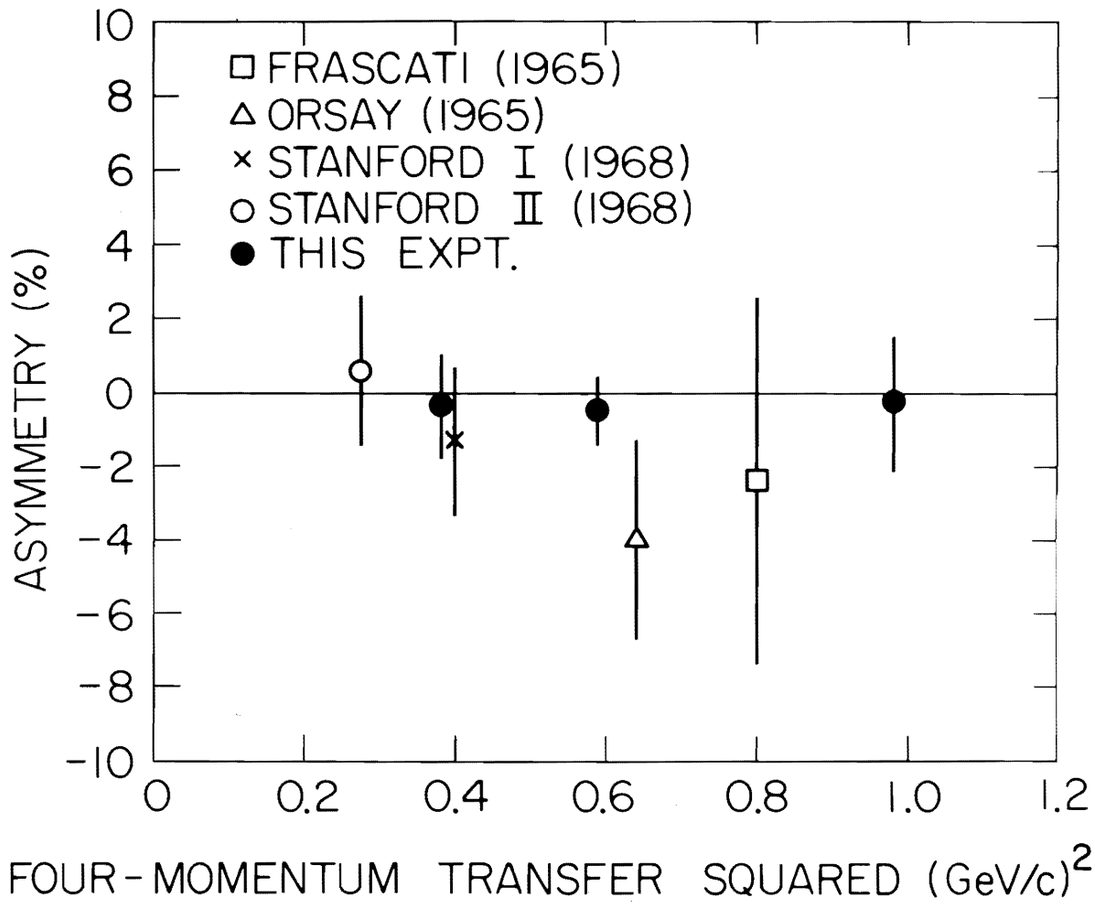
FRASCATI (1965)
ORSAY (1965)
STANFORD I (1968)
STANFORD II (1968)
THIS EXPT.
ASYMMETRY (%)
10
8
6
4
2
0
-2
-4
-6
-8
-10
0
0.2
0.4
0.6
0.8
1.0
1.2
FOUR-MOMENTUM TRANSFER SQUARED (GeV/c)^2

XBL 706-1081

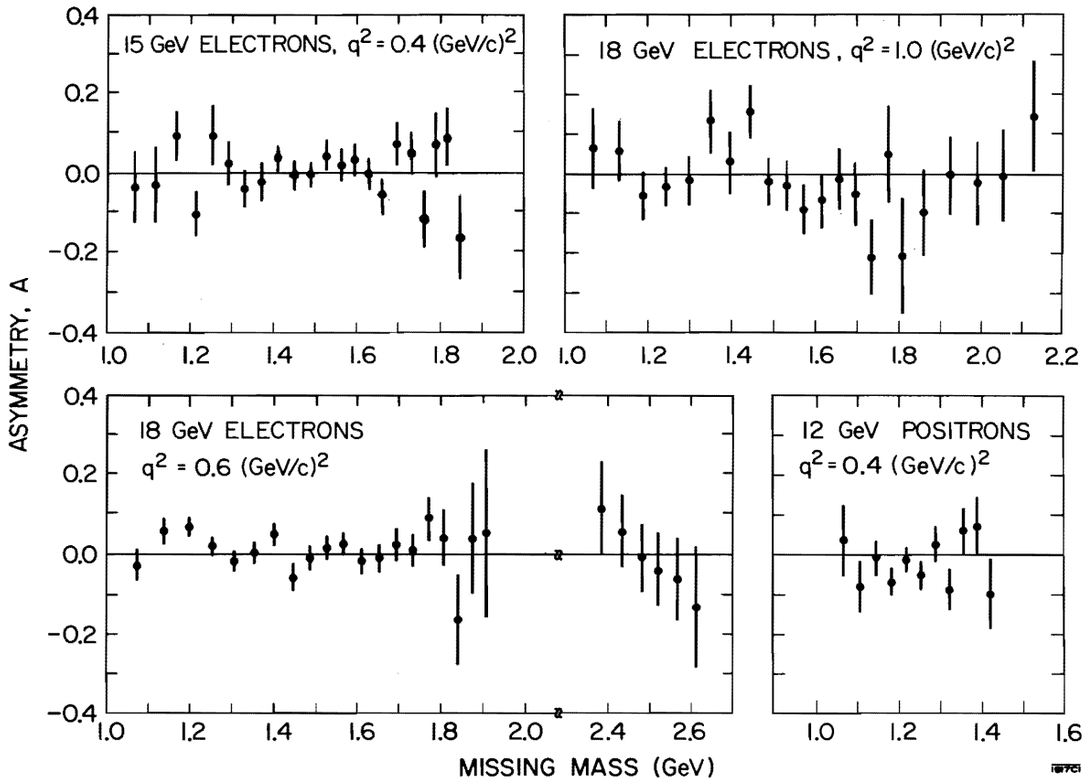
15 GeV ELECTRONS, $q^2 = 0.4$ (GeV/c)^2
18 GeV ELECTRONS, $q^2 = 1.0$ (GeV/c)^2
18 GeV ELECTRONS
$q^2 = 0.6$ (GeV/c)^2
12 GeV POSITRONS
$q^2 = 0.4$ (GeV/c)^2
ASYMMETRY, A
MISSING MASS (GeV)

XBL 708-1712

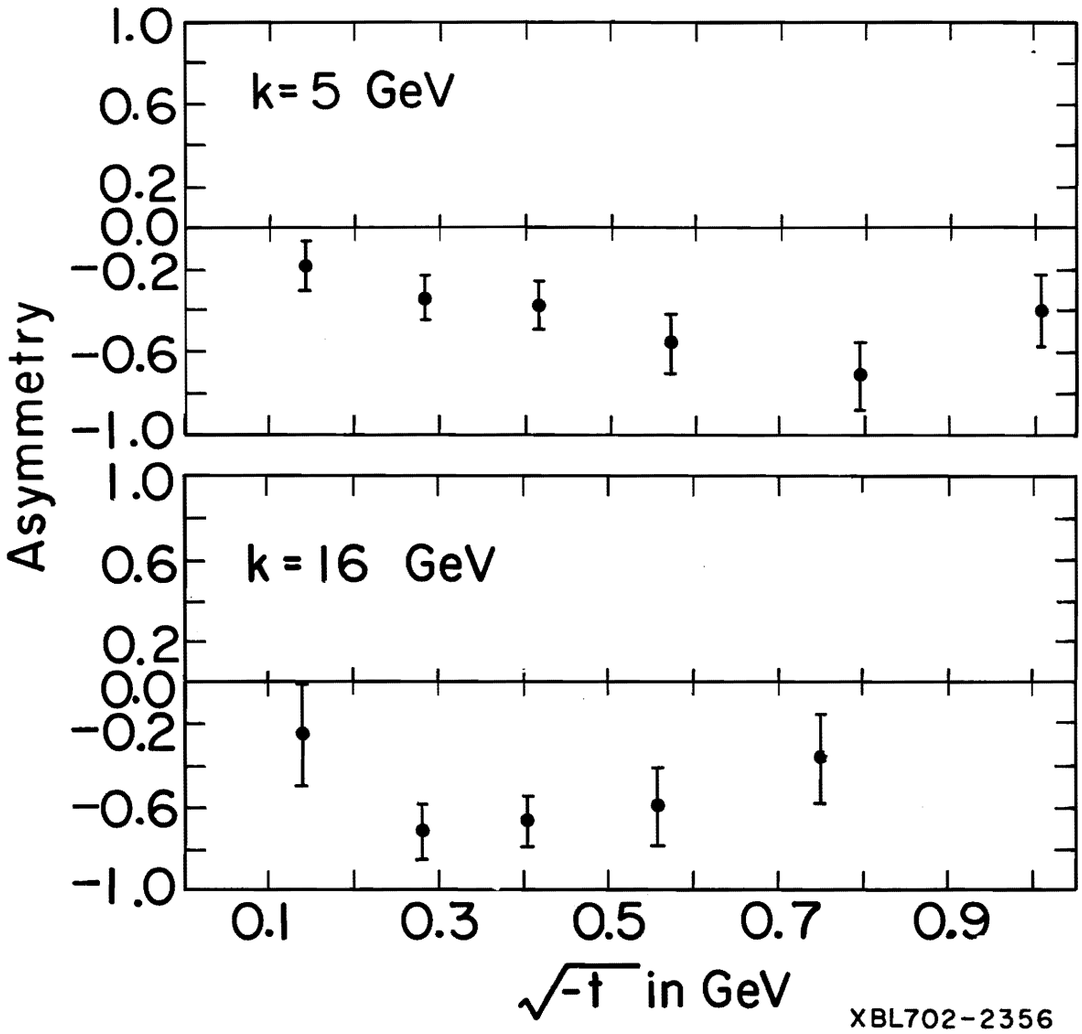
1.0
0.6
0.2
0.0
−0.2
−0.6
−1.0
k= 5 GeV
k = 16 GeV
Asymmetry
0.1
0.3
0.5
0.7
0.9
√-t in GeV
XBL702-2356

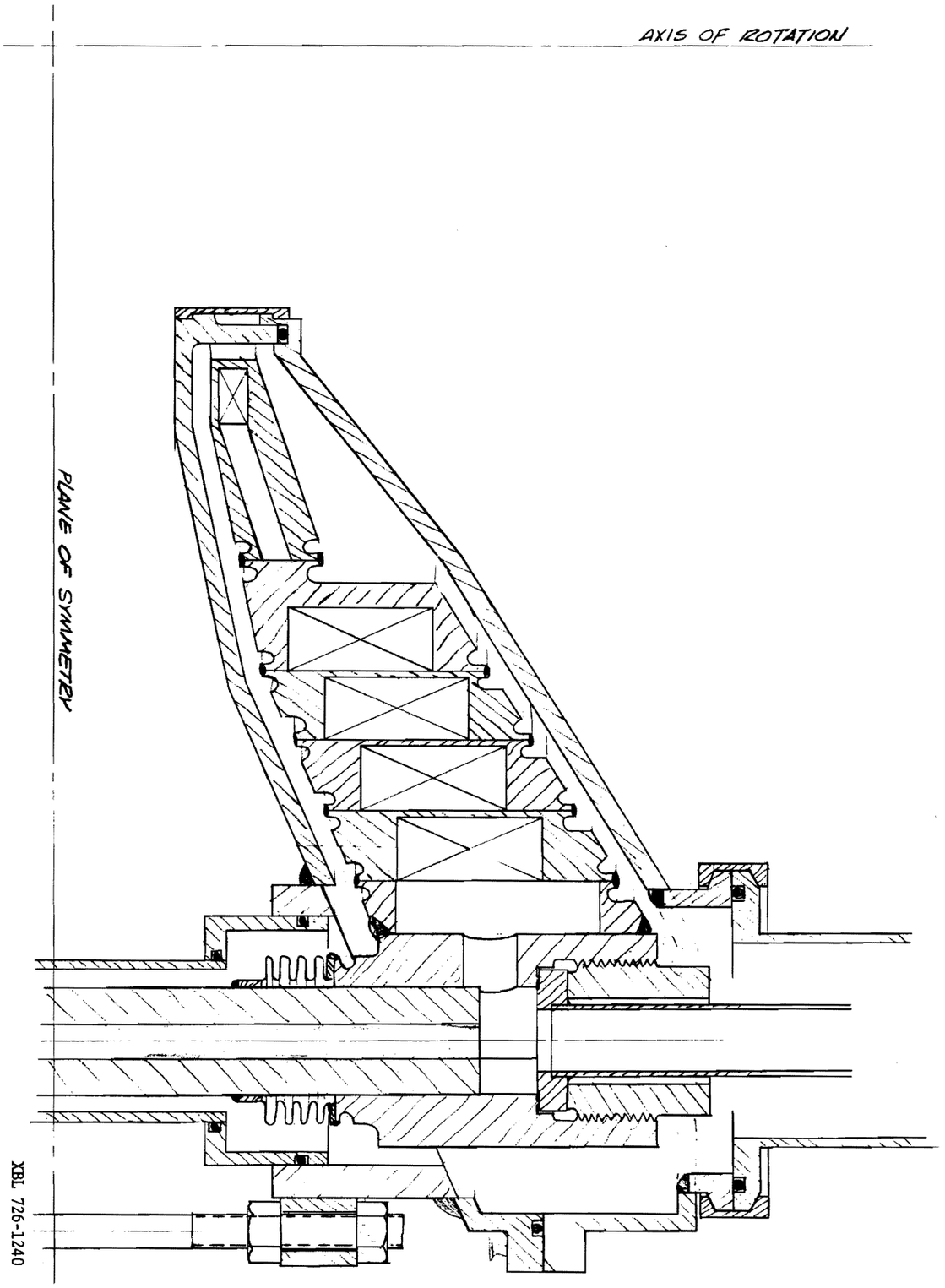
AXIS OF ROTATION
PLANE OF SYMMETRY
XBL 726-1240